Author Manuscript

Author Manuscript

Author Manuscript

Author Manuscript

HHS Public Access

Author manuscript

FASEB J. Author manuscript; available in PMC 2021 May 01.

Published in final edited form as:

FASEB J. 2020 May ; 34(5): 6999–7017. doi:10.1096/fj.201902710RR.

Lipid Rafts Are Required for Effective Renal D_1 Dopamine Receptor Function

Andrew C. Tiu, MD[1,†], **Jian Yang, PhD**[2,†], **Laureano D. Asico, DVM**[1], **Prasad Konkalmatt, PhD**[1], **Xiaoxu Zheng, MD, PhD**[1], **Santiago Cuevas, PhD**[1], **Xiaoyan Wang, MD, PhD**[1], **Hewang Li, PhD**[3], **Momina Mazhar**[1], **Robin A. Felder, PhD**[4], **Pedro A. Jose, MD, PhD**[1,5], **Van Anthony M. Villar, MD, PhD**[1]

[1]Division of Renal Diseases & Hypertension, Department of Medicine, The George Washington University School of Medicine & Health Sciences, Washington, DC 20052

[2]Department of Clinical Nutrition, The Third Affiliated Hospital of Chongqing Medical University. Chongqing 410020, P.R. China,

[3]Kidney Diseases Branch, National Institute of Diabetes and Digestive and Kidney Diseases, Bethesda, MD 20892,

[4]Department of Pathology, University of Virginia School of Medicine, Charlottesville, VA 22908,

[5]Department of Pharmacology/Physiology, The George Washington University School of Medicine & Health Sciences, Washington, DC 20052

Abstract

Effective receptor signaling is anchored on the preferential localization of the receptor in lipid rafts, which are plasma membrane platforms replete with cholesterol and sphingolipids. We hypothesized that the dopamine D_1 receptor (D_1R) contains structural features that allow it to reside in lipid rafts for its activity. Mutation of C347 palmitoylation site and Y218 of a newly identified Cholesterol Recognition Amino Acid Consensus motif resulted in the exclusion of D_1R from lipid rafts, blunted cAMP response, impaired sodium transport, and increased oxidative stress in renal proximal tubule cells. Kidney-restricted silencing of *Drd1* in C57BL/6J mice increased blood pressure (BP) that was normalized by renal tubule-restricted rescue with D_1R-wild-type but not the mutant D_1R-347A that lacks a palmitoylation site. Kidney-restricted disruption of lipid rafts by β-MCD jettisoned the D_1R from the brush border, decreased sodium excretion, and increased oxidative stress and BP in C57BL/6J mice. Deletion of the PX domain of the novel D_1R-binding partner sorting nexin 19 (SNX19) resulted in D_1R partitioning solely to non-raft domains,

Corresponding authors: 1) Andrew C. Tiu, MD, Einstein Medical Center, Department of Medicine, 5501 Old York Road, Philadelphia, PA, USA 19141, Phone: 1-917-754-4404, andrewchuatiu@yahoo.com.ph, tiuandre@einstein.edu, **2) Jian Yang, PhD**, Department of Clinical Nutrition, The Third Affiliated Hospital of Chongqing Medical University, Chongqing 410020, P.R. China., Phone: 023-60353438, jianyang@hospital.cqmu.edu.cn.

†AC Tiu and J Yang contributed equally and are considered as co-first authors

Author contributions

AT, JY: co-first authors; AT, JY, LD, VV: designed the research studies, conducted experiments, acquired data, and analyzed data, wrote manuscript; PK, XZ, SC, XW, MM: conducted experiments, acquired data, and analyzed data; PJ: analyzed data, and proofread manuscript.

Conflict of Interest

The authors have declared that no conflict of interest exists.

Author Manuscript Author Manuscript Author Manuscript Author Manuscript

while silencing of *SNX19* impaired D_1R function in renal proximal tubule cells. Kidney-restricted silencing of *Snx19* resulted in hypertension in C57BL/6J mice. Our results highlight the essential role of lipid rafts for effective D_1R signaling.

Keywords

dopamine receptors; lipid raft; blood pressure; sorting nexin 19 (SNX19); CRAC motif; palmitoylation; gene rescue

Introduction

Dopamine produced by renal proximal tubules, independent of renal nerves, engenders natriuresis through its cognate receptors by inhibiting the sodium pump and sodium transporters/exchangers (1–5). The dopamine receptors are classified as D_1-like (D_1R and D_5R) or D_2-like (D_3R, D_4R, and D_5R), depending on their coupling with stimulatory or inhibitory G proteins, $G\alpha_s$ or $G\alpha_i$, respectively. G protein-coupled receptor kinases (GRKs), especially GRK4, in the case of D_1R, are activated when dopamine receptors are stimulated leading to receptor phosphorylation, internalization, and desensitization (1–5). Dopamine accounts for more than 60% of renal Na^+ excretion during moderate volume expansion (3,4). Germline deletion of the *Drd1* gene in mice (*Drd1*$^{-/-}$) results in decreased sodium excretion and increased blood pressure (6).

The D_1R is expressed in both apical and basolateral membranes of the renal proximal tubule (RPT), especially in lipid raft microdomains and caveolae (7,8). Caveolae, a subset of lipid rafts, are small (60–80 nm) invaginations formed by the polymerization of caveolins (CAVs) with cholesterol (9). Lipid rafts are tightly packed, highly organized plasma membrane microdomains that are enriched in phospholipids, glycosphingolipids, and cholesterol (10,11). These abound in the apical and basolateral plasma membranes of polarized epithelial cells, such as renal proximal tubule cells. Lipid rafts form a semi-rigid structure composed of different proteins for effective GPCR signaling. Other functions of lipid rafts include the formation of platforms for extracellular matrix adhesion and intracellular cytoskeletal tethering to the plasma membrane. Caveolae are localized at the inner leaflet of the plasma membrane (9). Caveolae are found mostly at the basolateral membrane of renal epithelial cells that faces the blood supply; the basolateral membrane is most active during signal transduction (10–14). The renal D_1R partitions to the lipid raft/caveolae in human RPT cells (hRPTCs) and interact with the lipid raft protein marker CAV-1 (8,15) and CAV-2 (16), which are crucial in regulating D_1R turnover and signaling.

In this study, we tested the hypothesis that the renal D_1R must reside in specific microdomains, i.e., in lipid rafts, for its full activity. We demonstrate that the D_1R has critical structural determinants, such as the palmitoylation sites and the CRAC domain (17), which are essential for its targeting to and activity in lipid rafts. Kidney-restricted silencing of *Drd1* increases blood pressure in C57BL/6J mice that is normalized by renal tubule-restricted rescue with D_1R-wild-type but not the mutant D_1R-347A that lacks a D_1R palmitoylation site. Kidney-restricted disruption of lipid rafts by β-MCD jettisoned the D_1R from the brush border, decreased sodium excretion, and increased oxidative stress and blood

Author Manuscript Author Manuscript Author Manuscript Author Manuscript

pressure in C57BL/6J mice. The adaptor protein sorting nexin 19 (SNX19) is important in the palmitoylation, lipid raft microdomain localization, and function of renal D_1R. Silencing of *SNX19* inhibits D_1-like receptor-mediated inhibition of renal sodium transport and stimulation of cAMP production in human renal proximal tubule but not distal convoluted tubule cells. Kidney-restricted, siRNA-mediated, silencing of *Snx19* results in oxidative stress and elevated blood pressure in C57BL/6J mice.

Materials and Methods

Plasmid DNA Constructs and AAV Vectors

Human wild-type D_1R-WT (Accession: NM_000794, Clone ID: OHu23409C), ΔhD_1R-C347A, ΔhD_1R-C351A, and ΔhD_1R-Y218S and wild-type SNX19-WT (Accession: NM_014758) and ΔhSNX19-(-PX) were purchased from GenScript (Piscataway, NJ, USA). An upstream *Kpn*I restriction enzyme digestion site and a downstream *Bam*HI site were introduced into the respective genes by PCR. The PCR fragments were subcloned into the pcDNA3.1 vector with N-Myc (D_1R) or FLAG (SNX19) tag and sequenced which showed 100% fidelity. *E. coli* TOP10 strain was used for the DNA subcloning and expression of the plasmids.

The AAV vectors harboring hD_1R-WT (AAV-D_1R-WT) or the mutant ΔhD_1R-C347A (AAV-ΔhD_1R-C347A), with the expression controlled by a CMV promoter were constructed using the plasmid pAV-FH (Vigene Bioscience Inc., Rockville, MD, USA) as previously described (16,18,19).

Cell Culture and Transfection

Immortalized hRPTCs were generated from the normal portions of renal surgical specimens from normotensive Caucasian male patients who had renal cell carcinoma (8,15,20–22). Human embryonic kidney (HEK) 293 cells (ATCC, Manassas, VA, USA) and hRPTCs were maintained at 37°C in 95% air/5% CO_2 in DMEM/F-12 medium (Gibco, Grand Island, NY, USA) supplemented with 5% penicillin-streptomycin-amphotericin (Corning Life Sciences, Manassas, VA) and 10% FBS (Gibco, Grand Island, NY, USA). When 90% confluent, the cells were subcultured for use in experimental protocols using trypsin-EDTA (ThermoFisher; Rockford, IL, USA). The cells tested negative for *Mycoplasma* infection. Utilization of cells was limited to <25 passages to avoid the effects of cellular senescence. The cells were transfected with the plasmids using FuGENE® 6 (Cat# E2691; Promega, Madison, WI, USA) with a 3:1 reagent to plasmid DNA ratio. Stable transfection was done through treatment with 500 μg/μl of G418 (Invivogen, San Diego, CA, USA).

Cell Surface Biotinylation and Isolation

hRPTCs stably transfected with hD_1R-WT, ΔhD_1R-C347A, ΔhD_1R-C351A, ΔhD_1R-Y218S, and ΔhD_1R-LL were cultured in 10-cm dishes. The cells were washed with ice-cold PBS then incubated with 2 ml (500 μg/ml PBS) EZ-Link™ Sulfo-NHS-LC-LC-Biotin (Thermo Fisher Scientific, Rockford, IL, USA) at room temperature for 30 min. The cells were washed 3x with PBS and then 100 mM glycine. The cells were lysed with NP-40 Lysis Buffer (Amresco, Solon, OH, USA), containing Halt™ Protease and Phosphatase Inhibitor

Author Manuscript Author Manuscript Author Manuscript Author Manuscript

Single-Use Cocktail 1X (Thermo Fisher Scientific, Rockford, IL, USA). The protein concentration was measured using Pierce BCA Protein Assay Kit (Thermo Fisher Scientific, Rockford, IL, USA) to ensure uniform protein concentrations prior to immobilization with streptavidin. Washed Dynabeads™ MyOne™ Streptavidin T1 (Thermo Fisher Scientific, Rockford, IL, USA) magnetic beads were incubated with the biotinylated proteins in PBS for 30 min at room temperature, using gentle rotation. The beads were separated with a magnet for 2–3 min then washed 4–5x with PBS containing 0.1% BSA. The proteins were eluted with the Lane Marker Reducing Sample Buffer (5X) (Thermo Fisher Scientific, Rockford, IL, USA). The samples were heated at 60°C for 15 min, subjected to SDS-PAGE, and then immunoblotted with anti-N-Myc and anti-GGT antibody.

Lipid Raft Isolation and Sucrose Gradient Ultracentrifugation

The cells grown to confluence in 15-cm dishes were washed with PBS, scraped, pelleted, and centrifuged at ~800 x *g* for 1 min at 4°C. After discarding the supernatant, SPE Buffer I from the FOCUS™ SubCell kit (G-Biosciences, St Louis, MO, USA) was added to the pellet. The samples were vortexed and incubated on ice for 10 min. Then, the cells were lysed using a Dounce homogenizer with 20 strokes per sample. To pellet the nuclei, the samples were centrifuged at 700 x *g* for 10 min at 4°C. The supernatant was transferred to a new tube and subsequently centrifuged at 12,000 x *g* for 15 min at 4°C to pellet the mitochondria. The remaining supernatant was transferred to a new tube and subsequently centrifuged at 100,000 x *g* for 60 min at 4°C in a SW50.1 swinging bucket rotor (Beckman Coulter™, Palo Alto, CA, USA), to pellet the membrane fraction. The plasma membrane-enriched pellet was subjected to detergent-free sucrose gradient ultracentrifugation (16,23–26). Twelve fractions were collected and immunoblotted for N-Myc-tagged D_1R and CAV-1.

Western Blotting

Cell lysates were prepared on ice using Laemmli sample buffer (Bio-Rad; Hercules, CA) with a cocktail of Halt™ Protease and Phosphatase Inhibitors (Thermo Fisher Scientific, Rockford, IL, USA). The samples were heated at 60°C for 15 min. Proteins were resolved in 10% Criterion™ TGX™ Precast Midi Protein Gel (Bio-Rad; Hercules, CA, USA). The primary antibodies against N-Myc (Proteintech™, Rosemont, IL, USA), CAV-1 (Abcam, Cambridge, MA, USA), gamma-glutamyl transferase (GGT) (Genetex; Irvine, CA, USA), GODZ (Santa Cruz Biotechnology, Dallas, TX, USA), SERZ-β (Bioss Abs, Woburn, MA, USA), PPT-1 (Novus Biologicals, Centennial, CO), PTT-2 (Thermo Fisher Scientific, Rockford, IL, USA), GRK4 (Santa Cruz Biotechnology, Dallas, TX, USA), and SNX19 (ProteinTech, Rosemont, IL, USA) were prepared in an antibody diluent (Thermo Fisher Scientific, Rockford, IL, USA). The secondary antibodies, donkey anti-goat IgG-HRP (Santa Cruz Biotechnology, Dallas, TX, USA) and donkey anti-rabbit IgG-HRP (Santa Cruz Biotechnology, Dallas, TX, USA), were diluted with 5% non-fat dried milk. Hyperfilm ECL (GE Healthcare, Buckinghmanshire, UK) was used for western blotting detection. The bands were analyzed by ImageJ.

Co-Immunoprecipitation

Cell lysates were prepared on ice, using NP-40 lysis buffer (Thermo Fisher Scientific, Rockford, IL, USA) with a cocktail of Halt™ Protease and Phosphatase Inhibitors (Thermo

Author Manuscript Author Manuscript Author Manuscript Author Manuscript

Fisher Scientific, Rockford, IL, USA). Co-immunoprecipitation was carried out using DynaBeads Protein G (Thermo Fisher Scientific, Rockford, IL, USA), following the manufacturer's protocol. Normal rabbit or mouse IgG (Santa Cruz Biotechnology, Dallas, TX, USA) was used as negative control.

cAMP Measurement

The cells were cultured in 6-well plates in complete culture medium until they reached 90% confluence. The cells were serum-starved and pre-treated with the phosphodiesterase inhibitor IBMX (Millipore Aldrich, St. Louis, MO, USA) for 2 hr prior to treatment with fenoldopam monohydrobromide, 1 μM for 15 min at 37°C (Sigma Aldrich, St. Louis, MO, USA). Intracellular cAMP was measured using the Cyclic AMP Direct EIA Kit (Arbor Assays, Ann Arbor, MI, USA). The protein concentration of the samples was measured utilizing Pierce BCA Protein Assay Kit (Thermo Fisher Scientific, Rockford, IL, USA) to normalize cAMP levels. Data are expressed as mean ± standard error of the mean (pmol/mg protein/min) which was subsequently converted to % change of control.

Sodium Transport Studies

The cells were grown to confluence under polarized conditions on Polyester (PET) Membrane Transwell-Clear Inserts (Corning, Lowell, MA, USA) in 12-well plates. Transepithelial electrical resistance (TEER) using the Epithelial Voltohmmeter (EVOM) was used as a parameter to monitor the confluency of the cells. The cells were serum-starved for 2 hr and treated with vehicle, ouabain octahydrate 50 μM (Sigma Aldrich, St. Louis, MO, USA), fenoldopam monohydrobromide 1 μM, or the combination of fenoldopam and ouabain for 1 hr at the basolateral side. After washing the cells with PBS, 5 μl of DMSO and pluronic acid were mixed with Sodium Green™ Tetraacetate (Molecular Probes, Eugene, OR, USA). The cells were washed gently with PBS and the fluorescence emission was read in Victor II (excitation 485 nm and emission 535 nm). Protein concentration of the samples was also determined utilizing Pierce BCA Protein Assay Kit (Thermo Fisher Scientific, Rockford, IL, USA) to normalize the sodium levels. Results were reported as fluorescence units (reading from the Victor II)/mg protein and from these numbers, % of inhibition/activation was calculated.

Laser Scanning Confocal Microscopy

The cells were grown on poly-D-lysine-coated coverslips to 50% confluence. These were fixed for 20 min with 4% paraformaldehyde, permeabilized for 5 min with 0.05% Triton X-100, and immunostained using N-Myc and CAV-1 for 1 hr at room temperature. The cells were then treated with the appropriate fluorophore-conjugated secondary antibodies (Molecular Probes, Grand Island, NY, USA). To study the effect of inhibitors of palmitoylation on D_1R targeting to lipid rafts, the hRPTCs were pre-treated with 2-fluoropalmitic acid (Santa Cruz Biotechnology, Dallas, Texas, USA), 2-bromopalmitate (Millipore Aldrich, Louis, MO, USA), or cerulenin (Millipore Aldrich, Louis, MO, USA) at 37°C for 1 hr.

Immunohistochemistry of the mouse kidney samples was performed following standard protocol. The slides were deparaffinized in xylene at 60°C for 1 hr and then washed twice

Author Manuscript Author Manuscript Author Manuscript Author Manuscript

for 3 min in 100%, 95%, and 75% ethanol. The slides were boiled in sodium citrate buffer (pH 6.0) for 3 min under pressure for antigen retrieval, cooled to room temperature, and then blocked in 1% BSA for 30 min at room temperature. The sections were immunostained for *Cholera* toxin subunit B (CTxB), SNX19, GRK4, and D_1R, for 24 hr at 4°C. *Lotus tetragonolobus* lectin (LTL) conjugated with Alexa fluor® 647 was used to target the lectin-rich brush border and plasma membranes of the renal proximal tubules. DAPI was used to visualize the nuclei.

Confocal images of hRPTCs and kidney sections were obtained sequentially in separate channels to avoid bleed-through using a Carl Zeiss LSM 510 META with ×63/1.4 NA oil-immersion objective (Carl Zeiss, Thornwood, NY, USA) and processed using Zeiss 510 META with Physiology 3.5 and Multiple Time Series 3.5 software.

Intracellular ROS Detection

Intracellular ROS was quantified using the ROSstar™ 550 (Li-cor, Lincoln, NE, USA), which is a cell-permeable hydrocyanine probe that is initially non-fluorescent but becomes fluorescent after oxidation by ROS. It is specific for oxygen radicals, in particular for superoxide and hydroxyl radicals. Cultured RPTCs were treated with 50 μM of ROSstar 550. After incubation for 30 min at 37°C, the cells were washed 2X times with PBS and the fluorescence signal was quantified immediately by a plate reader at 540 nm excitation and 560 nm emission. The data were normalized by the protein concentration of each well.

Animal Care

Adult (8 wk-old) male C57BL/6J mice were obtained from Jackson Laboratory (Bar Harbor, ME, USA). The studies were conducted in accordance with U.S. National Institutes of Health guidelines for the ethical treatment and handling of animals in research and approved by the George Washington University Institutional Animal Care and Use Committee (IACUC). The mice were housed in a temperature-controlled facility with a 12:12-hr light-dark cycle and fed with mouse chow and water *ad libitum* for at least 2 wk before any studies were performed.

In Vivo β-MCD Infusion

Uninephrectomized adult male C57BL/6J mice on normal salt diet were given a 7-day renal subcapsular infusion of β-MCD (80 μg/kg/min) through an osmotic minipump. α-MCD or vehicle (PBS) was also infused in other mice as controls. On the day of the experiment, the mice were anesthetized with pentobarbital (50 mg/kg body weight, intraperitoneal) before cannulation of the femoral artery for blood pressure monitoring. A PE-90 catheter was also inserted through a cystotomy and exteriorized to collect urine for one hour. The remnant kidney was then perfused with 4% paraformaldehyde and collected for immunohistochemistry.

Telemetry

The mice were anesthetized with pentobarbital sodium (50 mg/kg, intraperitoneal). A transmitter (cat# TA11PA-C10, Data Sciences International) for mice was turned on magnetically 24 hr before and soaked in warm saline solution 10 min prior to the surgery

Author Manuscript Author Manuscript Author Manuscript Author Manuscript

(27). The catheter end was inserted into the temporarily occluded left carotid artery and the main body was secured in a skin pocket made by blunt dissection of the right flank of the animal. The incision was closed using 4–0 Ethilon®. Buprenorphine (0.05–0.10 mg/kg, intraperitoneal) was given to alleviate post-surgical pain. The mice were then closely observed and kept warm until ambulatory. The animals were then returned to the Animal Research Facility (ARF) telemetry room. Data were continuously collected and recorded through a dedicated computer running Dataquest. The mice were allowed to recover for 5–7 days to equilibrate the system in order to obtain accurate cardiovascular phenotyping. The mice were maintained on normal salt diet and were provided with unlimited access to drinking water.

Renal DRD1 and *SNX19* Gene Silencing and Renal *DRD1* Rescue

Uninephrectomized adult male C57BL/6J mice were anesthetized with pentobarbital (50 mg/kg, intraperitoneal) and placed on a heated board to maintain rectal temperature at 37°C. A polyethylene tube connected to an osmotic minipump (ALZET® Cupertino, CA, USA) was inserted underneath the renal capsule to deliver continuously the *Drd1*-specific siRNA or *Snx19*-specific siRNA (3 μg/day; Qiagen, Germantown, MD, USA) for 7 days. The siRNA was prepared in an *in vivo* transfection reagent (Mirus Bio, Madison, WI, USA) under sterile conditions. The tube was secured on top of the renal capsule using a drop of surgical glue, while the minipump was secured onto the abdominal wall by a suture. Infusion of vehicle or non-silencing mock siRNA (Qiagen, Germantown, MD, USA) served as controls.

On the 7^{th} day of siRNA infusion, blood pressure was measured under pentobarbital anesthesia using Cardiomax II to confirm the presence of elevated blood pressure. D_1R-WT and ΔD_1R-347A packaged in AAV9 vectors were infused into the renal tubules via the retrograde ureteral route, as described previously (18,19). Briefly, the distal portion of the ureter closest to the bladder and the renal artery supplying the target kidney were clamped off with micro-venous clips in pentobarbital-anesthetized mice. The ureter was then exposed and punctured with a 35-gauge needle to aspirate the urine. Using another syringe, 100 μL of the AAV vector (10^{11} viral genome particles) was injected retrogradely into the renal tubules via the ureter. The needle was withdrawn and the injection site on the ureter was clipped to prevent leakage. The arterial and the ureteral clips were kept in place for 30 min for maximum exposure to the infusate. The arterial and ureteral clips were then removed, and the abdominal contents were replaced in the proper order. The incision site was closed using a double layer of 6–0 ethilon absorbable sutures for the muscle and 6–0 silk sutures for the skin. The animals were allowed to recover and then returned to the ARF. On the 14^{th} day post-rescue, the mice were placed in metabolic cages for 24 hr to monitor for water and food consumption, as well as urine and fecal production. Urine Na^+ was measured using Easylyte® Analyser (Medica Corporation, Bedford, MA, USA). UNaV was calculated as urine volume × Na^+ (mEq/liter). The next day, the animals were anesthetized, and blood pressure was measured using Cardiomax II. The mice were sacrificed, and the blood, organs, and tissue samples were collected and stored accordingly for further experimentation.

Author Manuscript Author Manuscript Author Manuscript Author Manuscript

Statistics

Numerical data are expressed as mean ± standard error of the mean. Significant difference between 2 groups was determined by Student's *t*-test, while that among ≥3 groups was determined by one-way ANOVA followed by Holm-Sidak post-hoc test. Values of $P<0.05$ were considered significant. Statistical analysis was performed using SigmaStat 3.5 (Richmond, CA, USA).

Results

Structural Determinants of D_1R

Numerous post-translational modifications of proteins, such as palmitoylation of amino acid residues, serve as membrane anchors that promote lipid raft partitioning of several GPCRs (28). Palmitoylation is a process that involves the formation of thioesters between palmitate and cysteine residues, catalyzed by a family of palmitoyl acyltransferases to enhance the hydrophobicity of GPCRs (29). The C-terminus of D_1R possesses cysteine residues at positions C347 and C351, but not those at C297, C306, and C385, that undergo palmitoylation (30) (Figure 1).

We used the bioinformatics software CLC Main Workbench 7.7.2 (Qiagen) to identify a putative Cholesterol Recognition Amino Acid Consensus or CRAC motif, which is an ubiquitous and loosely defined sequence ([LV]-x(1,5)-Y-x(1,5)-[KR]) that has been shown to interact with cholesterol (17) and implicated in lipid raft partitioning (31). CRAC motifs are present in GPCRs, such as the rhodopsin receptor, β_2-adrenergic receptor, and serotonin$_{1A}$ receptor. The central tyrosine residue of the CRAC motif is critical for the cholesterol-binding property of the peripheral benzodiazepine and sigma-1 receptors. Substitution of tyrosine to serine impairs the receptors' ability to bind to cholesterol and partition to lipid rafts (17,32).

To determine if the D_1R palmitoylation sites and CRAC domain are critical for receptor function, we initially used PolyPhen-2 (http://genetics.bwh.harvard.edu/pph2/) to perform *ab initio* prediction of the possible effects of an amino acid substitution on the structure and function of a human protein, which predicted the 347A, 351A, and 218S mutations (CRAC motif Y>S) to be "probably damaging" (Figure 1).

D_1R Palmitoylation and SNX19

Palmitoylation is carried out at the Golgi by a DHHC (Asp-His-His-Cys) family of palmitoyl acyltransferases, such as the Golgi-specific DHHC zinc finger protein (GODZ) and, to a lesser extent, its paralog, the Sertoli cell gene with a zinc finger domain-β (SERZ-β) (33). We found that GODZ (55 kDa), but not SERZ-β, co-immunoprecipitated with the D_1R and GRK4 (Figure 2A). A higher band, conceivably representing the less enzymatically active GODZ dimers (34), co-immunoprecipitated with D_1R, GRK4, and sorting nexin 19 (SNX19). We also found that palmitoyl-protein thioesterase 1 (PPT-1), but not PPT-2, co-immunoprecipitated with the D_1R and GRK4 and may possibly be responsible for the removal of the palmitate from D_1R and GRK4 at the lysosomes (Figure 2A). GRK4 undergoes palmitoylation at C561 and C578 (35), which are important for its plasma

Author Manuscript Author Manuscript Author Manuscript Author Manuscript

membrane localization (36). SNX19 is a member of the sorting nexin family which plays a pivotal role in the molecular sorting of GPCRs, including the SNX5 for D_1R (37) and SNX1 for D_5R (38). We evaluated the subcellular distribution and colocalization of D_1R, GODZ, and SNX19 in hRPTCs via confocal microcopy and observed that in the basal state, they all colocalized at the perinuclear area, where the Golgi is located (Figure 2B). These results suggest the presence of an organized complex of enzyme (GODZ) and targeted substrates (D_1R and GRK4) that are conceivably held in place by a scaffold or adaptor protein (SNX19).

To determine if palmitoylation is crucial for the lipid raft targeting of the D_1R, we evaluated the colocalization of D_1R and the lipid raft marker CAV-1 in the presence or absence of pharmacological inhibitors of palmitoylation (Figure 2C). In the basal state, the D_1R was distributed in the cytoplasm and plasma membrane, where it colocalized with CAV-1. However, pre-treatment with the inhibitors of palmitoylation, i.e., 2-fluoropalmitate, 2-bromopalmitate (39), and cerulenin (40), limited the plasma membrane distribution of D_1R and CAV-1 and promoted their accumulation at the juxtanuclear area. The C-terminus of CAV-1 contains palmitoylation sites at C133, C144, and C156 (41) that are equally susceptible to the effects of the palmitoylation inhibitors.

D_1R mutants mistarget to the non-raft domains

Site-directed mutagenesis at ΔD_1R-347S did not interfere with the plasma membrane targeting of the receptor, as previously reported (42). We confirmed this observation by heterologously expressing the D_1R-wild-type (WT) and mutants (ΔD_1R-347A, ΔD_1R-351A, and ΔD_1R-218S) in hRPTCs and evaluating their distribution at the plasma membrane. The D_1R-WT and the D_1R mutants were found at the plasma membrane-enriched fraction, denoted by the plasma membrane marker gamma-glutamyl transferase (GGT) (Figure 3A). These observations were corroborated via confocal microscopy which showed the distribution and colocalization of D_1R-WT and the above mutants with the plasma membrane (Figure 3B). By contrast, the ΔD_1R-LL mutant remained mostly cytoplasmic in distribution, as previously reported (33).

We next evaluated the ability of D_1R-WT and mutants to segregate into the lipid raft microdomains. The receptors were heterologously expressed in hRPTCs and subjected to sucrose gradient ultracentrifugation to separate the more buoyant lipid rafts (fractions 1–6) from the less buoyant non-raft domains (fractions 7–12). The heterologously expressed D_1R-WT was distributed in both lipid raft and non-raft microdomains and to a greater extent in the latter than in the former region (Figure 4). By contrast, the D_1R mutants exclusively segregated to the non-raft microdomains.

D_1R mutants are dysfunctional

To determine the functional repercussions of the D_1R mutants which do not reside in lipid rafts, intracellular cAMP levels were measured in non-transfected and transfected cells that were treated with the D_1R/D_5R agonist fenoldopam or vehicle as control. There are no agonists that can distinguish the D_1R from the D_5R; D_1R and D_5R interact for a full response of either receptor, especially the D_1R-mediated stimulation of cAMP production

Author Manuscript Author Manuscript Author Manuscript Author Manuscript

(20). Agonist stimulation resulted in the expected increase in cAMP production in non-transfected (NT) and D_1R-WT cells, but not in cells expressing the D_1R mutants (Figure 5A). The overexpression of the mutant receptors somehow over-ride the response of the endogenous D_1R. The mutant receptors partition to non-raft domains leading to impaired function (cAMP production). Furthermore, this may be related, in part, to the increased production of reactive oxygen species in 218S and 347A (see below), when the D_1R function is impaired; the D_1R can inhibit the production of reactive oxygen species (3,5,25). Slightly higher basal cAMP levels were observed in cells expressing the ΔD_1R-347A and ΔD_1R-218S. Disruption of lipid rafts with methyl-β-cyclodextrin (β-MCD) increased the basal adenylyl cyclase activity but prevented the agonist-stimulated effect in hRPTCs that may be related to the presence of the adenylyl cyclase isoform targets (adenylyl cyclase 5 and 6) of D_1R in lipid rafts (23). We have suggested that lipid rafts keep adenylyl cyclase activity in a less active state in hRPTCs (24).

We next evaluated the effect of these receptors on sodium transport. In D_1R-WT cells, treatment with fenoldopam, which inhibits Na^+-K^+/ATPase (NKA) and sodium transporters/exchangers (3–6,8), or ouabain (a specific NKA inhibitor), or both at the basolateral side of polarized hRPTCs grown in Transwells, resulted in the expected increase in intracellular sodium because of inhibition of sodium egress from inside the cell to outside the cell via the basolateral membrane (Figure 5B). However, there was no increase in intracellular sodium concentration when cells expressing the mutant D_1R were stimulated with fenoldopam only, demonstrating the failure of the D_1R mutant receptors to inhibit the sodium pump. The inability of fenoldopam to inhibit sodium transport in cells expressing the mutant D_1R is probably related to its failure to produce signal transducers, such as cAMP and protein kinase A (3, 20). Ouabain alone or ouabain with fenoldopam was able to inhibit NKA in cells expressing the mutant D_1R, indicating the presence of a normally functional NKA in the cells with mutant D_1R.

Lipid raft disruption in C57BL/6J mouse kidney leads to hypertension and oxidative stress

To determine if our *in vitro* finding of impaired D_1R function due to mistargeting of D_1R mutants to the non-raft domains occurs *in vivo*, we infused β-MCD subcapsularly into the remnant kidney of uninephrectomized adult male C57BL/6J mice fed normal salt diet for 7 days. We observed an increase in the systolic blood pressure (SBP) in mice treated with β-MCD, but not in the control (vehicle- and α-MCD-treated) mice (Figure 6A). Sodium excretion (UNaV) was decreased in mice that received β-MCD, but not in control (vehicle- and α-MCD-treated) mice (Figure 6B).

We next evaluated the morphological changes that lipid raft disruption brought about to the renal parenchyma. While there were no gross changes in the structure of the renal proximal tubule, there was an almost complete disappearance of lipid rafts (denoted by the absence of *Cholera* toxin B [CTxB] staining) in the brush borders of renal proximal tubules (Figure 6C). Moreover, we also observed the redistribution of D_1R and SNX19 and, to a lesser extent, GRK4, from the brush borders to the cytoplasm, which may help explain the decreased sodium excretion and increased blood pressure in the β-MCD-treated mice.

Author Manuscript Author Manuscript Author Manuscript Author Manuscript

We next evaluated the presence of oxidative stress by measuring the levels of urinary isoprostanes (43) in β-MCD-treated mice and found that the urinary levels were increased compared with control (vehicle- and α-MCD-treated) mice (Figure 7A). Disruption of lipid rafts and lipid raft clustering is associated with oxidative stress in glomerular epithelial cells and hepatocytes (44–46) but not breast cancer cells. β-MCD facilitates the hepatoxicity of ochratoxin (46). Therefore, we further explored the role of lipid raft residency of D_1R on oxidative stress in mouse RPTCs and found that β-MCD treatment doubled the production of ROS in the treated cells, indicating the presence of heightened oxidative stress when the lipid rafts were perturbed (Figures 7B and 7C). Pre-treatment of the cells with diphenyleneiodonium (DPI, an inhibitor of NADPH oxidase or NOX) (36) abrogated the increase in ROS production in mouse RPTCs with disrupted lipid rafts, indicating the involvement of NOX in the oxidative stress (Figure 7C). To determine the involvement of D_1R and SNX19 in the development of oxidative stress, we silenced the endogenous expression of these proteins in mouse and human RPTCs and observed an increase in ROS production in both cell lines (Figures 7D and 7E, respectively), indicating the translational potential of our work. To ascribe directly the observed increase in oxidative stress to the D_1R mutants, we heterologously expressed the D_1R-WT and mutants in HEK-293 cells and observed a basal increase in ROS levels in cells expressing ΔD_1R-347A and ΔD_1R-218S, but not ΔD_1R-351A or D_1R-WT (Figure 7F). HEK-293 cells were used because these cells express negligible endogenous D_1R and D_5R (16,47).

Gene rescue with D_1R-WT normalized the hypertension in mice

Moreover, we performed renal tubular-restricted gene rescue in adult male C57BL/6J mice on normal salt diet that developed high blood pressure following renal-restricted silencing of renal *Drd1*. The increased blood pressure in renal D_1R-depleted mice was normalized by the renal tubule-restricted rescue with D_1R-WT but not ΔD_1R-347A mutant. The increase in blood pressure in the ΔD_1R-347A, relative to D_1R-WT, was observed at nighttime (Figure 8A, **bottom figure**) when the mice, being nocturnal animals, were mostly active. There was no difference in the expression levels of total D_1R or endogenous D_5R in the mice that were rescued with either D_1R-WT or D_1R-347A (Figure 8B).

Lipid raft disruption may or may not affect blood pressure and lipid raft disruption has effects other than that related to D_1R in the kidney (48–49). The role of CAV-1 in the regulation of blood pressure in mice has been inconsistent; germline deletion of *Cav-1* in mice has been shown to be associated with low, normal, or increased blood pressure (50–52). Therefore, we hypothesized that the D_1R is directed to lipid raft microdomains where it can interact with proteins important in D_1R signal transduction and function. SNX19 is a member of the sorting nexin family which plays a pivotal role in the molecular sorting of GPCRs, including the SNX5 for D_1R (37) and SNX1 for D_5R (38). As shown in Figure 2B, SNX19 and D_1R colocalize at the perinuclear area; they also colocalize in the plasma membrane, specifically in lipid raft, that is increased by fenoldopam treatment (Figure 9A). In another study, we found that treatment with fenoldopam beyond 5 minutes causes the internalization of D_1R and SNX19 (Figure 9B). In the basal state in the mouse kidney, the D_1R and SNX19 colocalize in the plasma membrane of mouse renal proximal tubules; the intravenous infusion of a dose of fenoldopam (2 μg/kg/min/5 min) does not affect blood

Author Manuscript Author Manuscript Author Manuscript Author Manuscript

pressure but increases the co-localization of D_1R and SNX19 in the cytosol of mouse renal proximal tubules (Figure 9C). Stimulated emission depletion (STED) microscopy confirmed the colocalization of D_1R and SNX19 in mouse renal proximal tubules (Figure 9D).

There is specificity of the D_1R and SNX19 interaction because D_1R but not D_5R as the immunoprecipitant, co-immunoprecipitated with SNX19 in mouse renal proximal tubule cells (Figure 10A). Reverse co-immunoprecipitation shows that SNX19, not SNX13 or SNX25, co-immunoprecipitated with D_1R (Figure 10B).

We next determined if SNX19 is required for the lipid raft targeting of D_1R by expressing a mutant SNX19 [ΔSNX19-(-PX)] in which the PX domain has been deleted and thus, cannot target the plasma membrane. The PX domain is a phosphoinositide-binding domain that is involved in targeting a protein to the lipid rafts of the plasma membrane (53). In the presence of the SNX19-WT, the **endogenous** D_1R partitioned mainly to the lipid raft (Figure 11). However, the expression of ΔSNX19-(-PX) resulted in the mistargeting of decreased levels of endogenous D_1R to the non-raft fractions. Endogenous SNX19-WT is mainly found in lipid rafts. These results underscore the importance of the D_1R palmitoylation sites for lipid raft targeting that may be mediated by SNX19.

To corroborate the crucial role of SNX19 on the lipid raft localization and activity of D_1R in hRPTCs, we studied the effect of the D_1-like receptor agonist, fenoldopam (1 μM/15 min) on cAMP production in hRPTCs and human distal convoluted tubule cells and on sodium transport in hRPTCs in which *SNX19* is silenced using siRNA (Figure 12). Silencing *SNX19* decreased the fenoldopam-mediated increase in cAMP production in hRPTCs but not in human distal convoluted tubule cells. The impairment in fenoldopam-mediated increase in cAMP production in hRPTCs was accompanied by the abrogation of the ability of fenoldopam to inhibit basolateral sodium transport.

As further evidence for the importance of SNX19 on the homeostatic regulation of blood pressure by renal D_1R, we also performed renal-restricted silencing of *Snx19*, similar to that performed for D_1R (Figure 8). siRNA-mediated knockdown of renal *Snx19* increased the systolic blood pressure of C57BL/6J mice on normal salt diet (0.8% NaCl) (Figure 13). This increase in blood pressure was accompanied by a decrease in the expression of renal D_1R.

Discussion

Our current study shows that the D_1R has several intrinsic features that allow it to reside in lipid rafts. The D_1R has two palmitoylation sites at C347 and C351 (30) and a single putative CRAC motif (current study), which when mutated (but not 351A) results in D_1R dysfunction, leading to blunted cAMP response, impaired sodium excretion, and increased oxidative stress. Additionally, the D_1R contains a C-terminal di-Leu (L344+L345) motif that is important for its plasma membrane trafficking (42); however, its role in lipid raft partitioning has not been explored. The D_1R also contains a “CAV binding motif” in transmembrane domain 7 (7). Decreased CAV-1 expression in hRPTCs leads to the uncoupling of D_1R from adenylyl cyclase, reduced association of NKA with adaptor protein-2, internalization of NKA (8), and reduced D_1-like receptor-mediated inhibition of

Author Manuscript Author Manuscript Author Manuscript Author Manuscript

Na^+ transport (11). Renal-restricted silencing of *Cav-1* expression with siRNA or renal-restricted disruption of lipid rafts with β-MCD decreases sodium excretion and produces hypertension in sodium-loaded rats (11) and mice on a normal salt diet (current study). By contrast, global *Cav-1* knockout mice have either low (50) or normal (51) blood pressure. However, the low or normal blood pressure in mice with germline (global) deletion of *Cav-1* has been related to heart failure and increased generation of nitric oxide from eNOS (51–55). The germline deletion of *Cav-1* in mice fed a high salt diet slightly but non-significantly increased blood pressure that was aggravated by nitric oxide inhibition with N^G-nitro-L-arginine methyl ester to a greater extent in *Cav-1*$^{-/-}$ than *Cav-1*$^{+/+}$ mice (54). The difference in the blood pressure between renal-restricted silencing of *Cav-1* and germline deletion of *Cav-1* (51,52,54,55) or vascular smooth muscle-restricted deletion (53), could be due to organ/tissue/cell specificity of the effects of lipid rafts, or genes for that matter.

Other intrinsic properties of the D_1R may favor its partitioning to the lipid rafts. Overall, the hydrophobicity score calculated via GPMAWlite (https://www.alphalyse.com/customer-support/gpmaw-lite-bioinformatics-tool/start-gpmaw-lite) for D_1R is +0.33 compared with those of the interleukin 4 receptor α (−0.33) and CD71 (−0.23), which mainly reside in non-raft domains (56,57). The more positive the value, the more hydrophobic are the component amino acids, and the more miscible the protein or transmembrane is to the hydrophobic regions of the plasma membrane. As was suspected, the hydrophobicity scores for the 7 transmembrane domains of D_1R are +2.23, +1.89, +1.61, +1.84, +1.20, +2.02, and +0.66. The transmembrane length may also favor lipid raft partitioning. The D_1R transmembrane domains are 24-amino acid residues long, which is the average length for long transmembranes that prefer the plasma raft membrane. Reducing the number from 24 to 18 amino acid residues markedly decreases the raft partition coefficient (58).

The importance of both the palmitoylation process and the presence of the CRAC motif on the dopamine receptors are underscored by our studies and those by others. Jensen et al. showed that C347, but not C351, is critical in human D_1R function and plasma membrane expression in COS-7 cells (59). However, Kong et al. showed that the palmitoylation of D_1R is not essential for the localization of D_1R in caveolae (60). There are three major differences in the former and our studies. First, Kong et al. used double-mutant D_1R (347A +351A), while we used single-mutant D_1R (347A or 351A). Second, their experiments were performed in SV40-transformed COS-7 cells, which are fibroblast-like cells from the African green monkey kidney, in contrast to our studies which were performed using fully differentiated, hTERT-immortalized RPTCs from humans. Third, they performed detergent-free sucrose gradient fractionation on whole cell lysates, which include intracellular membranes, while we performed detergent-free sucrose gradient centrifugation on plasma membrane-enriched fractions (13). In a subsequent report, Kong et al reported that “constitutive palmitoylation may serve to stabilize the D_1R during agonist-dependent caveolar internalization” (60).

Mutation of the palmitoylation sites or the CRAC motif resulted in D_1R dysfunction. A higher basal cAMP production was observed in the presence of the D_1R mutants, similar to the results observed upon the disruption of lipid rafts (24). The exclusion of these mutants from the lipid rafts may have prevented the inhibitory effect of the lipid raft protein CAV-1

Author Manuscript Author Manuscript Author Manuscript Author Manuscript

on $G\alpha_s$ and/or facilitated GTP binding (61). Alternatively, these mutations may have changed the basal conformation of the receptor into a constitutively active version (62) by locking the receptor in either a high affinity “agonist conformation” or low affinity “antagonist conformation” (63). In contrast to our current and published (40) results which showed an impairment of cAMP production in response to the D_1R/D_5R-specific agonist fenoldopam among the mutant D_1Rs, Jin et al. reported that D_1R palmitoylation mutants had normal adenylyl cyclase activity in response to dopamine (61). The difference in our results may result from their use of: intact cells (*vs.* isolated plasma membranes in our studies) to measure adenylyl cyclase activity (*vs.* intracellular cAMP levels); dopamine (the natural ligand for all of the dopamine receptor isoforms, *vs.* fenoldopam, which is more specific for D_1R/D_5R (64)); and baby hamster kidney cells *vs.* adult hRPTCs.

Our study demonstrates that disruption of the lipid raft via cholesterol depletion, siRNA-mediated silencing of *Drd1* or *Snx19* genes, or *Drd1* C347A and Y218S mutations result in increased oxidative stress in RPTCs or C57BL/6J mice. Lipid raft bestows protection against oxidative stress by maintaining NOX in the inactive state in hRPTCs (24), the opposite of what is observed in normotensive rat RPTCs (65). However, RPTCs from hypertensive rats have greater basal oxidase activity conceivably due to greater NOX2 and Rac1 abundance in their lipid rafts (65). Agonist stimulation of D_1R may directly regulate the level of ROS through its interaction with NOX and paraoxonase 2 (PON2) (25) and nuclear factor E2-related factor 2 (66). The absence of increased ROS levels and basal cAMP production when ΔD_1R-351A is expressed is reminiscent of Jensen et al’s findings that it is mainly the ΔD_1R-C347 mutant that is impaired functionally (59). The ability of fenoldopam, through the D_1R/D_5R, to inhibit NOX activity is, in part, due to its ability to increase cAMP production, via a PKC and PKA crosstalk (67). However, while ΔD_1R-351A was able to prevent the ability of fenoldopam to increase cAMP and inhibit basolateral sodium transport, its ability to decrease ROS production persisted. This could be due to the ability of D_1R to stimulate antioxidant enzymes such as superoxide dismutase, glutathione peroxidase, glutamyl cysteine transferase, and heme-oxygenase 1, independent of cAMP. Indeed, the ability of D_1R and D_5R to stimulate PON2 activity is related, in part, to its translocation to non-raft domains (25).

We have demonstrated that disruption of lipid rafts via β-MCD impairs the localization of renal D_1R in the brush borders of proximal tubules, resulting in decreased sodium excretion and high blood pressure in mice on normal salt diet, similar to the results by Gildea et al in rats (11). In our study, the concomitant decrease in brush border distribution of SNX19 and GRK4 may conceivably contribute to the D_1R dysfunction. The activity of the sodium transporters and NKA may also be directly affected by raft disruption since they are mostly lipid raft-bound (68). The crucial role of the C347 palmitoylation site was corroborated by our gene rescue studies; renal tubule-restricted rescue with *DRD1-WT* but not *DRD1-347A* mutant, subcloned in AAV vectors, normalized the blood pressure at day 21 in the mice with renal-restricted silencing of *Drd1*. The siRNA-mediated renal-restricted *Drd1* knockdown mouse model was used in lieu of the *Drd1* knockout mice because we wanted to eliminate non-renal factors in the process.

Author Manuscript Author Manuscript Author Manuscript Author Manuscript

SNX19 is normally exclusively found in the lipid raft and may be an additional, extrinsic factor that ensures the subsequent lipid raft partitioning of D_1R. It may serve as a hub that provides an entropic advantage and promotes the effective interaction between D_1R and the GODZ enzyme, resulting in D_1R palmitoylation and lipid raft distribution (15–17,23). Unlike SNX1 and SNX5, SNX19 only possesses the canonical PX domain but not the Bin/Amphiphysin/Rvs (BAR) domain, which is a dimerization and membrane-curvature sensing module (69). It is conceivable that the ability of SNX19 to foster the partitioning of D_1R to the lipid raft may reside in the PX domain, in the absence of the BAR domain, since the PX domain is important in protein localization in lipid rafts (70). Lipid raft targeting is not specific to D_1R but probably needs SNX19 to target it to lipid rafts, ensuring D_1R specificity. Deletion of the PX domain of SNX19 prevents the targeting of D_1R to lipid rafts and renal-restricted silencing of *Snx19* in mice increases blood pressure. Moreover, SNX19 regulates the renal expression of D_1R but not D_5R, the other D_1-like dopamine receptor.

In summary, renal D_1R requires lipid raft residency for its full functionality (signal transduction), which includes increase in cAMP production, inhibition of sodium transport, inhibition of ROS production, and blood pressure homeostasis (Figure 14). SNX19 acts as an adaptor or scaffold protein for the palmitoylation of renal D_1R required for lipid raft targeting.

Perspectives

Disruption of lipid rafts is implicated in renal diseases such as glomerulosclerosis, lupus nephritis, and unilateral ureteropelvic junction obstruction (12,71,72) and other cardiovascular diseases such as heart failure, myocardial infarction, and pulmonary hypertension (73). Lipid rafts are important in dopamine function via the D_1R. Abnormal D_1R signaling is involved in the pathogenesis of renal disease and hypertension. Thus, it is important to evaluate the dynamics among the various components of the D_1R signaling clusters in the lipid rafts of renal tubule cells. Moreover, other determinants of lipid raft partitioning such as CARC motif, GXXG motif, tilted domain, CAV-binding motif, and N-linked myristoylation of glycine residues in the D_1R should be studied to determine their biological relevance to D_1R-mediated regulation of renal function and blood pressure.

Acknowledgments

The work was funded by grants from the US National Institutes of Health, P01HL074940, R01HL092196, R37HL023081, R01DK039308, DK090918, and R01DK119652. It was also supported partly by minigrants (VA Villar & LD Asico) from the National Kidney Foundation of Maryland (NKF-MD), and Key Program of The Third Affiliated Hospital of Chongqing Medical University (KY19024).

Abbreviations:

AAV	adeno-associated virus
ANOVA	analysis of variance
ARF	animal research facility
BCA	bicinchoninic acid

Author Manuscript Author Manuscript Author Manuscript Author Manuscript

β-MCD	methyl-beta-cyclodextrin
cAMP	cyclic adenosine monophosphate
CAV	caveolin
CRAC motif	cholesterol recognition/interaction amino acid consensus
co-IP	co-immunoprecipitation
CTxB	Cholera Toxin subunit B
DAPI	diamino phenylindole
D_1R	dopamine 1 receptor
GPCR	G protein-coupled receptor
DMEM/F-12	Dulbecco's Modified Eagle Medium/Nutrient Mixture F-12
GGT	gamma-glutamyl transferase
GAPDH	glyceraldehyde 3-phosphate dehydrogenase
hTERT	human telomerase reverse transcriptase
GODZ	Golgi-associated DHHC-type zinc finger protein
GRK4	GPCR kinase 4
LTL	*Lotus tretragonolobus* lectin
NKA	sodium/potassium-ATPase
NOX	NADPH oxidase
PPT1/2	palmitoyl-protein thioesterase 1/2
PON2	paraoxonase 2
RPTCs	renal proximal tubule cells
ROS	reactive oxygen species
siRNA	short, interfering RNA
SNX19	sorting nexin 19
SERZ-β	sertoli cell gene with a zinc finger domain-β
STED	Stimulated Emission Depletion Microscopy
UNaV	urinary sodium excretion
WT	wild-type

Author Manuscript Author Manuscript Author Manuscript Author Manuscript

References

1. Pinto V, Pinho MJ, Soares-da-Silva P (2013) Renal amino acid transport systems and essential hypertension. FASEB J. 27(8):2927–38 [PubMed: 23616567]
2. Gurevich EV, Gainetdinov RR, Gurevich VV (2016) G protein-coupled receptor kinases as regulators of dopamine receptor functions. Pharmacol Res. 111:1–16 [PubMed: 27178731]
3. Armando I, Villar VA, Jose PA (2011) Dopamine and renal function and blood pressure regulation. Compr Physiol. 1(3):1075–117 [PubMed: 23733636]
4. Harris RC (2012) Abnormalities in renal dopamine signaling and hypertension: the role of GRK4. Curr Opin Nephrol Hypertens. 21(1):61–5 [PubMed: 22123211]
5. Banday AA, Fazili FR, Lokhandwala MF (2007) Oxidative stress causes renal dopamine D1 receptor dysfunction and hypertension via mechanisms that involve nuclear factor-kappaB and protein kinase C. J Am Soc Nephrol. 18(5):1446–57. [PubMed: 17409305]
6. Albrecht FE, Drago J, Felder RA, Printz MP, Eisner GM, Robillard JE, Sibley DR, Westphal HJ, Jose PA (1996) Role of the D1A dopamine receptor in the pathogenesis of genetic hypertension. J Clin Invest. 97(10):2283–8 [PubMed: 8636408]
7. Kong MM, Hasbi A, Mattocks M, Fan T, O'Dowd BF, George SR (2007) Regulation of D1 dopamine receptor trafficking and signaling by caveolin-1. Mol Pharmacol.72(5):1157–70 [PubMed: 17699686]
8. Gildea JJ, Israel JA, Johnson AK, Zhang J, Jose PA, Felder RA (2009) Caveolin-1 and dopamine-mediated internalization of NaKATPase in human renal proximal tubule cells. Hypertension. 54(5):1070–6. [PubMed: 19752292]
9. Anderson RG, Jacobson K (2002) A role for lipid shells in targeting proteins to caveolae, rafts, and other lipid domains. Science. 296(5574):1821–5 [PubMed: 12052946]
10. Lingwood D, Simons K (2010) Lipid rafts as a membrane-organizing principle. Science. 327(5961):46–50 [PubMed: 20044567]
11. Gildea JJ, Kemp BA, Howell NL, Van Sciver RE, Carey RM, Felder RA (2011) Inhibition of renal caveolin-1 reduces natriuresis and produces hypertension in sodium-loaded rats. Am J Physiol Renal Physiol. 300(4):F914–20 [PubMed: 21289050]
12. Vallés PG, Manucha W, Carrizo L, Vega Perugorria J, Seltzer A, Ruete C (2007) Renal caveolin-1 expression in children with unilateral ureteropelvic junction obstruction. Pediatr Nephrol. 22(2):237–48 [PubMed: 17111160]
13. Villar VA, Cuevas S, Zheng X, Jose PA (2016) Localization and signaling of GPCRs in lipid rafts. Methods Cell Biol. 132:3–23 [PubMed: 26928536]
14. Simons K, Toomre D (2000) Lipid rafts and signal transduction. Nat Rev Mol Cell Biol. 1(1):31–9. [PubMed: 11413487]
15. Gildea JJ, Israel JA, Johnson AK, Zhang J, Jose PA, Felder RA (2009) Caveolin-1 and dopamine-mediated internalization of NaKATPase in human renal proximal tubule cells. Hypertension. 54(5):1070–6 [PubMed: 19752292]
16. Yu P, Yang Z, Jones JE, Wang Z, Owens SA, Mueller SC, Felder RA, Jose PA. (2004) D1 dopamine receptor signaling involves caveolin-2 in HEK-293 cells. Kidney Int. 66(6):2167–80 [PubMed: 15569306]
17. Jamin N, Neumann JM, Ostuni MA, Vu TK, Yao ZX, Murail S, Robert JC, Giatzakis C, Papadopoulos V, Lacapère JJ (2005) Characterization of the cholesterol recognition amino acid consensus sequence of the peripheral-type benzodiazepine receptor. Mol Endocrinol. 19(3):588–94 [PubMed: 15528269]
18. Konkalmatt PR, Asico LD, Zhang Y, Yang Y, Drachenberg C, Zheng X, Han F, Jose PA, Armando I (2016) Renal rescue of dopamine D2 receptor function reverses renal injury and high blood pressure. JCI Insight. 1(8)pii:e85888 [PubMed: 27358912]
19. Asico LD, Cuevas S, Ma X, Jose PA, Armando I, Konkalmatt PR (2018) Nephron segment-specific gene expression using AAV vectors. Biochem Biophys Res Commun. 497(1):19–24 [PubMed: 29407172]

Author Manuscript Author Manuscript Author Manuscript Author Manuscript

20. Gildea JJ, Shah IT, Van Sciver RE, Israel JA, Enzensperger C, McGrath HE, Jose PA, Felder RA (2014) The cooperative roles of the dopamine receptors, D1R and D5R, on the regulation of renal sodium transport. Kidney Int. 86(1):118–26 [PubMed: 24552847]
21. Felder RA, Sanada H, Xu J, Yu PY, Wang Z, Watanabe H, Asico LD, Wang W, Zheng S, Yamaguchi I, Williams SM, Gainer J, Brown NJ, Hazen-Martin D, Wong LJ, Robillard JE, Carey RM, Eisner GM, Jose PA (2002) G protein-coupled receptor kinase 4 gene variants in human essential hypertension. Proc Natl Acad Sci USA. 99(6):3872–7 [PubMed: 11904438]
22. Gildea JJ, Xu P, Kemp BA, Carlson JM, Tran HT, Bigler Wang D, Langouët-Astrié CJ, McGrath HE, Carey RM, Jose PA, (2018) Felder RA. Sodium bicarbonate cotransporter NBCe2 gene variants increase sodium and bicarbonate transport in human renal proximal tubule cells. PLoS One. 13(4):e0189464 [PubMed: 29642240]
23. Yu P, Sun M, Villar VA, Zhang Y, Weinman EJ, Felder RA, Jose PA (2014) Differential dopamine receptor subtype regulation of adenylyl cyclases in lipid rafts in human embryonic kidney and renal proximal tubule cells. Cell Signal. 26(11): 2521–9 [PubMed: 25049074]
24. Han W, Li H, Villar VA, Pascua AM, Dajani MI, Wang X, Natarajan A, Quinn MT, Felder RA, Jose PA, Yu P (2008) Lipid rafts keep NADPH oxidase in the inactive state in human renal proximal tubule cells. Hypertension. 51(2):481–7 [PubMed: 18195159]
25. Yang S, Yang Y, Yu P, Yang J, Jiang X, Villar VA, Sibley DR, Jose PA, Zeng C (2015) Dopamine D1 and D5 receptors differentially regulate oxidative stress through paraoxonase 2 in kidney cells. Free Radic Res. 49(4):397–410 [PubMed: 25740199]
26. Yu P, Villar VA, Jose PA (2013) Methods for the study of dopamine receptors within lipid rafts of kidney cells. Methods Mol Biol. 964:15–24 [PubMed: 23296775]
27. Butz GM, Davisson RL (2001) Long-term telemetric measurement of cardiovascular parameters in awake mice: a physiological genomics tool. Physiol Genomics. 5(2):89–97 [PubMed: 11242593]
28. Levental I, Lingwood D, Grzybek M, Coskun U, Simons K (2010) Palmitoylation regulates raft affinity for the majority of integral raft proteins. Proc Natl Acad Sci USA. 107(51):22050–4 [PubMed: 21131568]
29. Lorent JH, Levental I (2015) Structural determinants of protein partitioning into ordered membrane domains and lipid rafts. Chem Phys Lipids.192:23–32 [PubMed: 26241883]
30. Jin H, Xie Z, George SR, O'Dowd BF (1999) Palmitoylation occurs at cysteine 347 and cysteine 351 of the dopamine D(1) receptor. Eur J Pharmacol. 386(2–3):305–12 [PubMed: 10618483]
31. Schwarzer R, Levental I, Gramatica A, Scolari S, Buschmann V, Veit M, Herrmann A (2014) The cholesterol-binding motif of the HIV-1 glycoprotein gp41 regulates lateral sorting and oligomerization. Cell Microbiol. 16(10):1565–81 [PubMed: 24844300]
32. Palmer CP, Mahen R, Schnell E, Djamgoz MB, Aydar E (2007) Sigma-1 receptors bind cholesterol and remodel lipid rafts in breast cancer cell lines. Cancer Res. 67(23):11166–75 [PubMed: 18056441]
33. Fang C, Deng L, Keller CA, Fukata M, Fukata Y, Chen G, Lüscher B (2006) GODZ-mediated palmitoylation of GABA(A) receptors is required for normal assembly and function of GABAergic inhibitory synapses. J Neurosci. 26(49):12758–68 [PubMed: 17151279]
34. Lai J, Linder ME. (2013) Oligomerization of DHHC protein S-acyltransferases. J Biol Chem. 288(31):22862–70 [PubMed: 23793055]
35. Premont RT, Macrae AD, Stoffel RH, Chung N, Pitcher JA, Ambrose C, Inglese J, MacDonald ME, Lefkowitz RJ (1996) Characterization of the G protein-coupled receptor kinase GRK4. Identification of four splice variants. J Biol Chem. 271(11):6403–10 [PubMed: 8626439]
36. Gildea JJ, Huang Z, Wang DB, Tran H, Felder RA (2014) GRK4 palmitoylation is necessary for membrane association and dopamine-1 receptor activity. Hypertension. 64(Suppl 1):A532
37. Villar VA, Armando I, Sanada H, Frazer LC, Russo CM, Notario PM, Lee H, Comisky L, Russell HA, Yang Y, Jurgens JA, Jose PA, Jones JE (2013) Novel role of sorting nexin 5 in renal D(1) dopamine receptor trafficking and function: implications for hypertension. FASEB J. 27(5):1808–19 [PubMed: 23195037]
38. Villar VA, Jones JE, Armando I, Asico LD, Escano CS Jr, Lee H, Wang X, Yang Y, Pascua-Crusan AM, Palmes-Saloma CP, Felder RA, Jose PA (2013) Sorting nexin 1 loss results in D5 dopamine

Author Manuscript Author Manuscript Author Manuscript Author Manuscript

receptor dysfunction in human renal proximal tubule cells and hypertension in mice. J Biol Chem. 288(1):152–63 [PubMed: 23152498]

39. Ebersole B, Petko J, Woll M, Murakami S, Sokolina K, Wong V, Stagljar I, Lüscher B, Levenson R (2015) Effect of C-Terminal S-Palmitoylation on D2 Dopamine Receptor Trafficking and Stability. PLoS One. 10(11):e0140661 [PubMed: 26535572]
40. Zheng B, Zhu S, Wu X (2015) Clickable analogue of cerulenin as chemical probe to explore protein palmitoylation. ACS Chem Biol. 10(1):115–21 [PubMed: 25322207]
41. Dietzen DJ, Hastings WR, Lublin DM (1995) Caveolin is palmitoylated on multiple cysteine residues. Palmitoylation is not necessary for localization of caveolin to caveolae. J Biol Chem. 270:6838–6842 [PubMed: 7896831]
42. Guo Y, Jose PA (2011) C-terminal di-leucine motif of dopamine D_1 receptor plays an important role in its plasma membrane trafficking. PLoS One. 6(12):e29204 [PubMed: 22206002]
43. Milne GL, Musiek ES, Morrow JD (2005) F2-isoprostanes as markers of oxidative stress in vivo: an overview. Biomarkers. 10 Suppl 1:S10–23 [PubMed: 16298907]
44. Boini KM, Zhang C, Xia M, Han WQ, Brimson C, Poklis JL, Li PL (2010) Visfatin-induced lipid raft redox signaling platforms and dysfunction in glomerular endothelial cells. Biochim Biophys Acta. 1801(12):1294–304 [PubMed: 20858552]
45. Aliche-Djoudi F, Podechard N, Collin A, Chevanne M, Provost E, Poul M, Le Hégarat L, Catheline D, Legrand P, Dimanche-Boitrel MT, Lagadic-Gossmann D, Sergent O (2013) A role for lipid rafts in the protection afforded by docosahexaenoic acid against ethanol toxicity in primary rat hepatocytes. Food Chem Toxicol. 60:286–96 [PubMed: 23907024]
46. Zhang Y, Qi X, Zheng J, Luo Y, Zhao C, Hao J, Li X, Huang K, Xu W (2016) Lipid Rafts Disruption Increases Ochratoxin A Cytotoxicity to Hepatocytes. J Biochem Mol Toxicol. 30(2):71–9 [PubMed: 26861962]
47. Wang Q, Jolly JP, Surmeier JD, Mullah BM, Lidow MS, Bergson CM, Robishaw JD (2001) Differential dependence of the D1 and D5 dopamine receptors on the G protein gamma 7 subunit for activation of adenylyl cyclase. J Biol Chem 276: 39386–93 [PubMed: 11500503]
48. Riquier AD, Lee DH, McDonough AA (2009) Renal NHE3 and NaPi2 partition into distinct membrane domains. Am J Physiol Cell Physiol. 296(4):C900–10 [PubMed: 19158399]
49. Yoon MS, Won KJ, Kim DY, Hwang DI, Yoon SW, Jung SH, Lee KP, Jung D, Choi WS, Kim B, Lee HM (2015) Diminished Lipid Raft SNAP23 Increases Blood Pressure by Inhibiting the Membrane Fluidity of Vascular Smooth-Muscle Cells. J Vasc Res. 52(5):321–33 [PubMed: 26930561]
50. Murata T, Lin MI, Huang Y, Yu J, Bauer PM, Giordano FJ, Sessa WC (2007) Reexpression of caveolin-1 in endothelium rescues the vascular, cardiac, and pulmonary defects in global caveolin-1 knockout mice. J Exp Med. 204:2373–82 [PubMed: 17893196]
51. Desjardins F, Lobysheva I, Pelat M, Gallez B, Feron O, Dessy C, Balligand JL (2008) Control of blood pressure variability in caveolin-1-deficient mice: role of nitric oxide identified in vivo through spectral analysis. Cardiovasc Res. 79:527–36 [PubMed: 18349137]
52. Pojoga LH, Yao TM, Sinha S, Ross RL, Lin JC, Raffetto JD, Adler GK, Williams GH, Khalil RA (2008) Effect of dietary sodium on vasoconstriction and eNOS-mediated vascular relaxation in caveolin-1-deficient mice. Am J Physiol Heart Circ Physiol. 294(3):H1258–6 [PubMed: 18178722]
53. DeLalio LJ, Keller AS, Chen J, Boyce AKJ,, Artamonov MV, Askew-Page HR, Keller TCS, Johnstone SR, Weaver RB, Good ME, Murphy SA,, Best AK, Mintz EL, Penuela S, Greenwood IA, Machado RF, Somlyo AV, Swayne LA, Minshall RD, Isakson BE (2018). Interaction Between Pannexin 1 and Caveolin-1 in Smooth Muscle Can Regulate Blood Pressure. Arterioscler Thromb Vasc Biol. 38(9):2065–78. [PubMed: 30026274]
54. Wunderlich C, Schober K, Schmeisser A, Heerwagen C, Tausche AK, Steinbronn N, Brandt A, Kasper M, Schwencke C, Braun-Dullaeus RC, Strasser RH (2008) The adverse cardiopulmonary phenotype of caveolin-1 deficient mice is mediated by a dysfunctional endothelium. J Mol Cell Cardiol. 44:938–47 [PubMed: 18417152]
55. Pojoga LH, Adamová Z, Kumar A, Stennett AK, Romero JR, Adler GK, Williams GH, Khalil RA (2010) Sensitivity of NOS-dependent vascular relaxation pathway to mineralocorticoid receptor

Author Manuscript Author Manuscript Author Manuscript Author Manuscript

blockade in caveolin-1-deficient mice. Am J Physiol Heart Circ Physiol. 298:H1776–88 [PubMed: 20363891]

56. Kim YH, Ninomiya Y, Yamashita S, Kumazoe M, Huang Y, Nakahara K, Won YS, Murata M, Fujimura Y, Yamada K, Tachibana H (2014) IL-4 receptor α in non-lipid rafts is the target molecule of strictinin in inhibiting STAT6 activation. Biochem Biophys Res Commun. 450(1):824–30 [PubMed: 24960198]
57. Huang YS, Chiang NY, Hu CH, Hsiao CC, Cheng KF, Tsai WP, Yona S, Stacey M, Gordon S, Chang GW, Lin HH (2012) Activation of myeloid cell-specific adhesion class G protein-coupled receptor EMR2 via ligation-induced translocation and interaction of receptor subunits in lipid raft microdomains. Mol Cell Biol. 32(8):1408–20 [PubMed: 22310662]
58. Diaz-Rohrer BB, Levental KR, Simons K, Levental I (2014) Membrane raft association is a determinant of plasma membrane localization. Proc Natl Acad Sci USA. 111(23):8500–5. [PubMed: 24912166]
59. Jensen AA, Pedersen UB, Kiemer A, Din N, Andersen PH (1995) Functional importance of the carboxyl tail cysteine residues in the human D1 dopamine receptor. J Neurochem. 65:1325–31 [PubMed: 7643110]
60. Kong MM, Verma V, O'Dowd BF, George SR (2011) The role of palmitoylation in directing dopamine D1 receptor internalization through selective endocytic routes. Biochem Biophys Res Commun. 405(3):445–9 [PubMed: 21241663]
61. Jin H, Zastawny R, George SR, O'Dowd BF (1997) Elimination of palmitoylation sites in the human dopamine D1 receptor does not affect receptor-G protein interaction. Eur J Pharmacol. 324(1):109–16 [PubMed: 9137920]
62. Ostrom RS, Insel PA (2004) The evolving role of lipid rafts and caveolae in G protein-coupled receptor signaling: implications for molecular pharmacology. Br J Pharmacol. 143(2):235–45 [PubMed: 15289291]
63. Sensoy O, Weinstein H (2015) A mechanistic role of Helix 8 in GPCRs: Computational modeling of the dopamine D2 receptor interaction with the GIPC1-PDZ-domain. Biochim Biophys Acta. 1848(4):976–83 [PubMed: 25592838]
64. http://www.guidetopharmacology.org/GRAC/ObjectDisplayForward?objectId=214
65. Li H, Han W, Villar VA, Keever LB, Lu Q, Hopfer U, Quinn MT, Felder RA, Jose PA, Yu P (2009) D1-like receptors regulate NADPH oxidase activity and subunit expression in lipid raft microdomains of renal proximal tubule cells. Hypertension. 53(6):1054–61 [PubMed: 19380616]
66. Cuevas S, Yang Y, Konkalmatt P, Asico LD, Feranil J, Jones J, Villar VA, Armando I, Jose PA (2015) Role of nuclear factor erythroid 2-related factor 2 in the oxidative stress-dependent hypertension associated with the depletion of DJ-1. Hypertension. 65(6):1251–7 [PubMed: 25895590]
67. Yu P, Han W, Villar VA, Li H, Arnaldo FB, Concepcion GP, Felder RA, Quinn MT, Jose PA (2011) Dopamine D1 receptor-mediated inhibition of NADPH oxidase activity in human kidney cells occurs via protein kinase A-protein kinase C cross talk. Free Radic Biol Med. 50(7):832–40 [PubMed: 21193028]
68. Welker P, Geist B, Frühauf JH, Salanova M, Groneberg DA, Krause E, Bachmann S (2007) Role of lipid rafts in membrane delivery of renal epithelial Na+-K+-ATPase, thick ascending limb. Am J Physiol Regul Integr Comp Physiol. 292(3):R1328–37 [PubMed: 17082358]
69. Peter BJ, Kent HM, Mills IG, Vallis Y, Butler PJ, Evans PR, McMahon HT (2004) BAR domains as sensors of membrane curvature: the amphiphysin BAR structure. Science. 303(5657):495–9 [PubMed: 14645856]
70. Mas C, Norwood SJ, Bugarcic A, Kinna G, Leneva N, Kovtun O, Ghai R, Ona Yanez LE, Davis JL, Teasdale RD, Collins BM Structural basis for different phosphoinositide specificities of the PX domains of sorting nexins regulating G-protein signaling. J Biol Chem. 289(41):28554–68
71. Zhang C, Hu JJ, Xia M, Boini KM, Brimson C, Li PL (2010) Redox signaling via lipid raft clustering in homocysteine-induced injury of podocytes. Biochim Biophys Acta. 1803(4):482–91 [PubMed: 20036696]
72. Deng GM, Tsokos GC (2008) Cholera toxin B accelerates disease progression in lupus-prone mice by promoting lipid raft aggregation. J Immunol. 181(6):4019–26 [PubMed: 18768857]

Author Manuscript Author Manuscript Author Manuscript Author Manuscript

73. Fridolfsson HN, Patel HH (2013) Caveolin and caveolae in age associated cardiovascular disease. J Geriatr Cardiol. 10(1):66–74 [PubMed: 23610576]

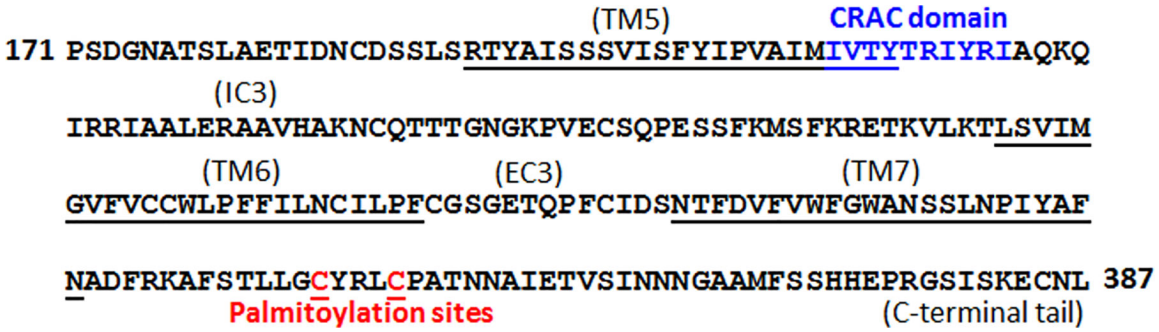

Figure 1. Partial primary sequence (171–387 a.a. residues) of the human D_1R.

The palmitoylation sites, Cholesterol Recognition Amino Acid Consensus (CRAC) domain, and boundaries of the transmembrane domains (TM, underlined), extracellular (EC) and intracellular (IC) domains, and the C-terminal tail are indicated.

Author Manuscript Author Manuscript Author Manuscript Author Manuscript

Author Manuscript Author Manuscript Author Manuscript Author Manuscript

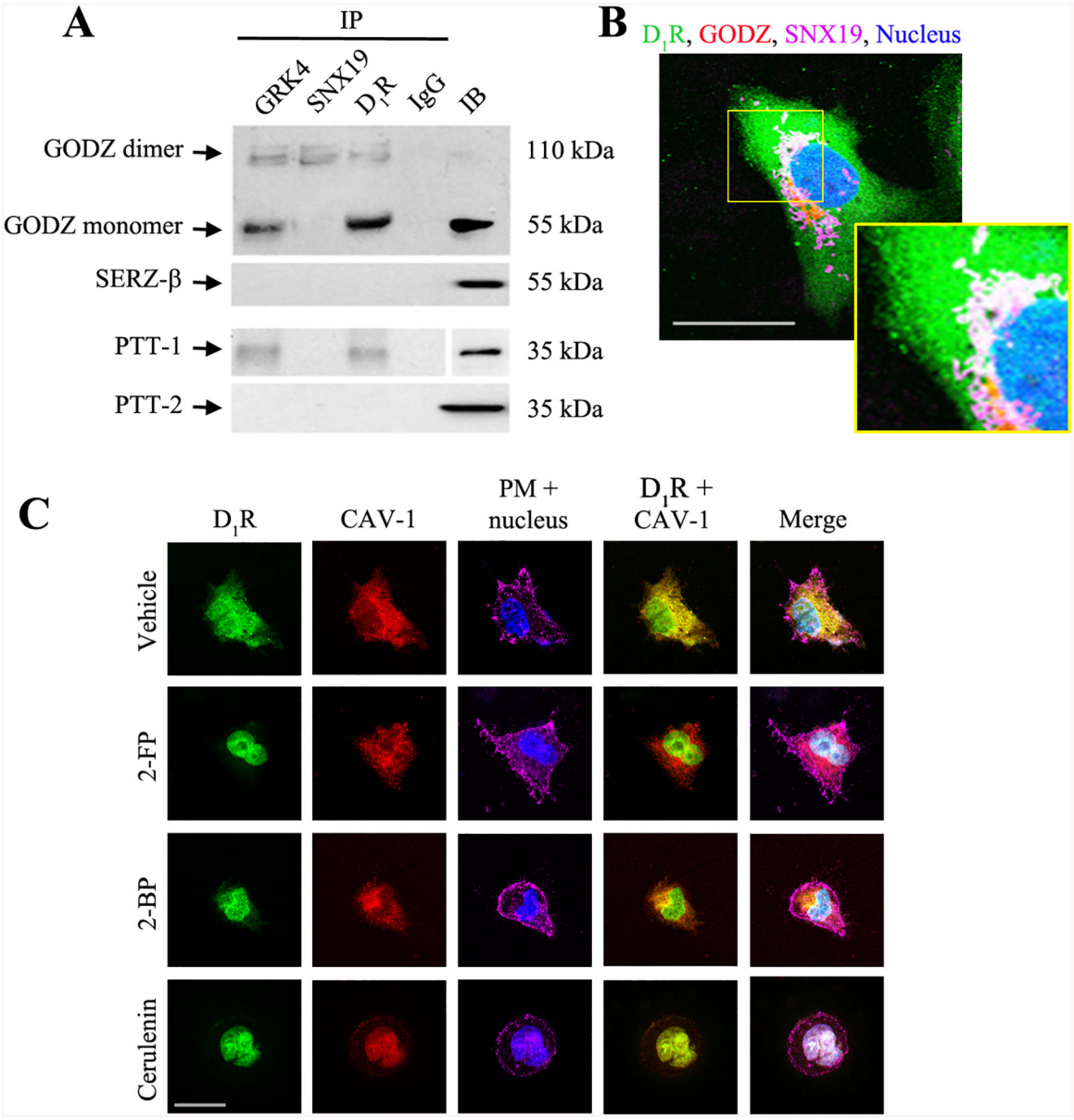

Figure 2. Interaction of endogenous D_1R, SNX19, GRK4, GODZ, and caveolin-1 (CAV-1).

A. Co-immunoprecipitation (IP) of D_1R, SNX19, and GRK4 with GODZ and palmitoyl-protein thioesterase 1 (PPT-1) and PPT-2 at the basal state. Normal rabbit IgG was used as negative control and regular immunoblot (IB) of the cell lysate was used as positive control. Results of 1 of 3 experiments are shown. **B:** Basal distribution D_1R (pseudocolored green), SNX19 (pseudocolored magenta), and GODZ (pseudocolored red) at the perinuclear area in serum-starved hRPTCs. Colocalization of all three is denoted by the discrete white areas. DAPI was used to visualize the nucleus (pseudocolored blue). 630x magnification, scale bar = 10 μm. **C:** Serum-starved hRPTCs were pre-treated with palmitoylation inhibitors 2-fluoropalmitate (2-FP), 2-bromopalmitate (2-BP), or cerulenin for 2 hr, or vehicle as control. Basal colocalization of D_1R (pseudocolored green) and CAV-1 (pseudocolored red) is indicated by the discrete yellow areas in the D_1R + CAV-1 image of vehicle-treated cells.

Author Manuscript Author Manuscript Author Manuscript Author Manuscript

Wheat germ agglutinin and DAPI were used to visualize the plasma membrane and nucleus (pseudocolored magenta and blue), respectively. 630x magnification, scale bar = 20 μm. Representative images are shown from 1 of 3 experiments. About 20–30 cells were scored per treatment.

Author Manuscript Author Manuscript Author Manuscript Author Manuscript

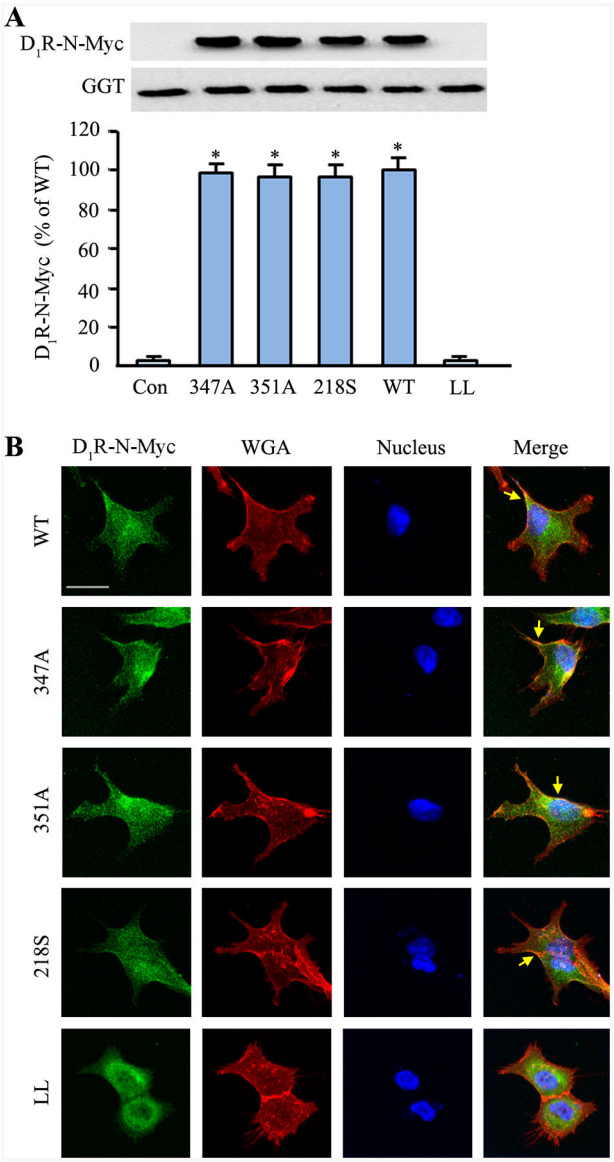

Figure 3. D_1R mutants are targeted to the plasma membrane but not the lipid raft.

hRPTCs were transfected with the N-Myc-tagged D_1R-WT or mutants (347A, 351A, 218S, and LL). The ΔD_1R-LL is a dileucine mutant that does not target the plasma membrane (42) and was used as an additional control to non-transfected hRPTCs. **A:** Total cell lysates were collected, and plasma membrane proteins were extracted via biotinylation and isolation. The heterologously expressed D_1R was immunoblotted, using anti-Myc, and γ-glutamyl-transferase (GGT) as loading control. **B:** hRPTCs were grown on cover slips, transfected with the N-Myc-tagged D_1R-WT or mutants, and grown to 50% confluence prior to fixation, double immunostaining, mounting, and confocal microscopy. An anti-Myc antibody was used to visualize the N-Myc-tagged D_1R (pseudocolored green). Wheat germ agglutinin (WGA) was used to visualize the plasma membrane (pseudocolored red), and DAPI to visualize the nuclei (pseudocolored blue). Basal colocalization of the D_1R with the plasma

membrane is denoted by the discrete yellow areas (yellow arrows) in the merged images. 630x magnification, scale bar = 10 μm

Author Manuscript Author Manuscript Author Manuscript Author Manuscript

Author Manuscript Author Manuscript Author Manuscript Author Manuscript

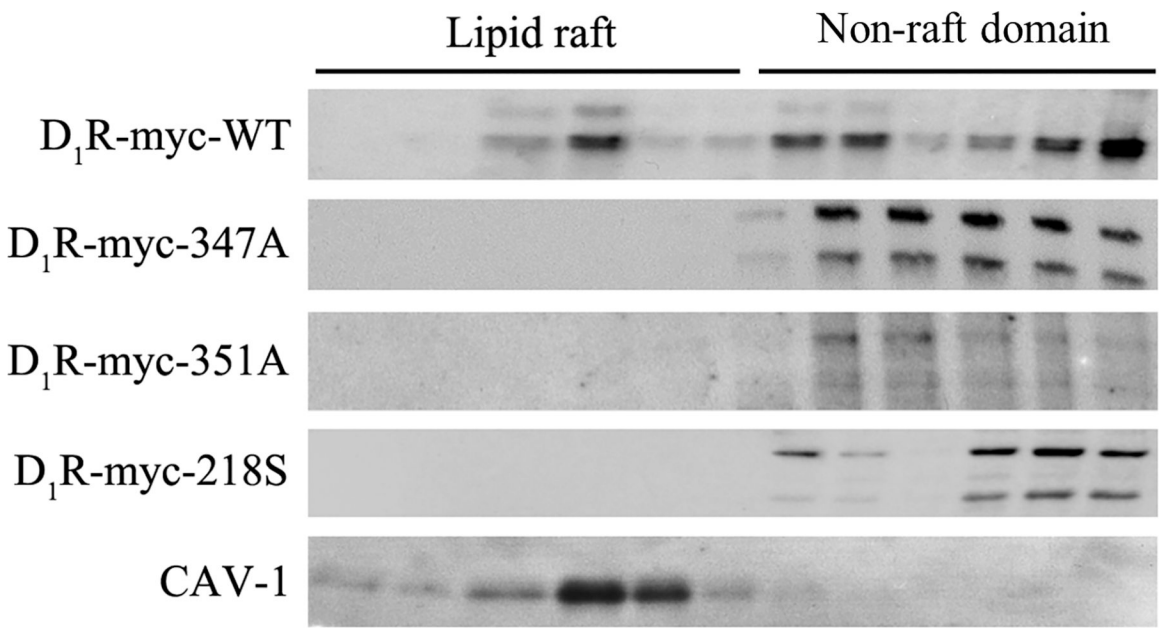

Figure 4. Lipid raft distribution of D_1R-WT and mutants.

A: Plasma membrane-enriched fractions were prepared and subjected to detergent-free sucrose gradient ultracentrifugation and the 12 fractions were immunoblotted for N-Myc which was used to tag the D_1Rs. Caveolin-1 (CAV-1) was used as the lipid raft marker. Immunoblots from 1 of 3 experiments is shown.

Author Manuscript Author Manuscript Author Manuscript Author Manuscript

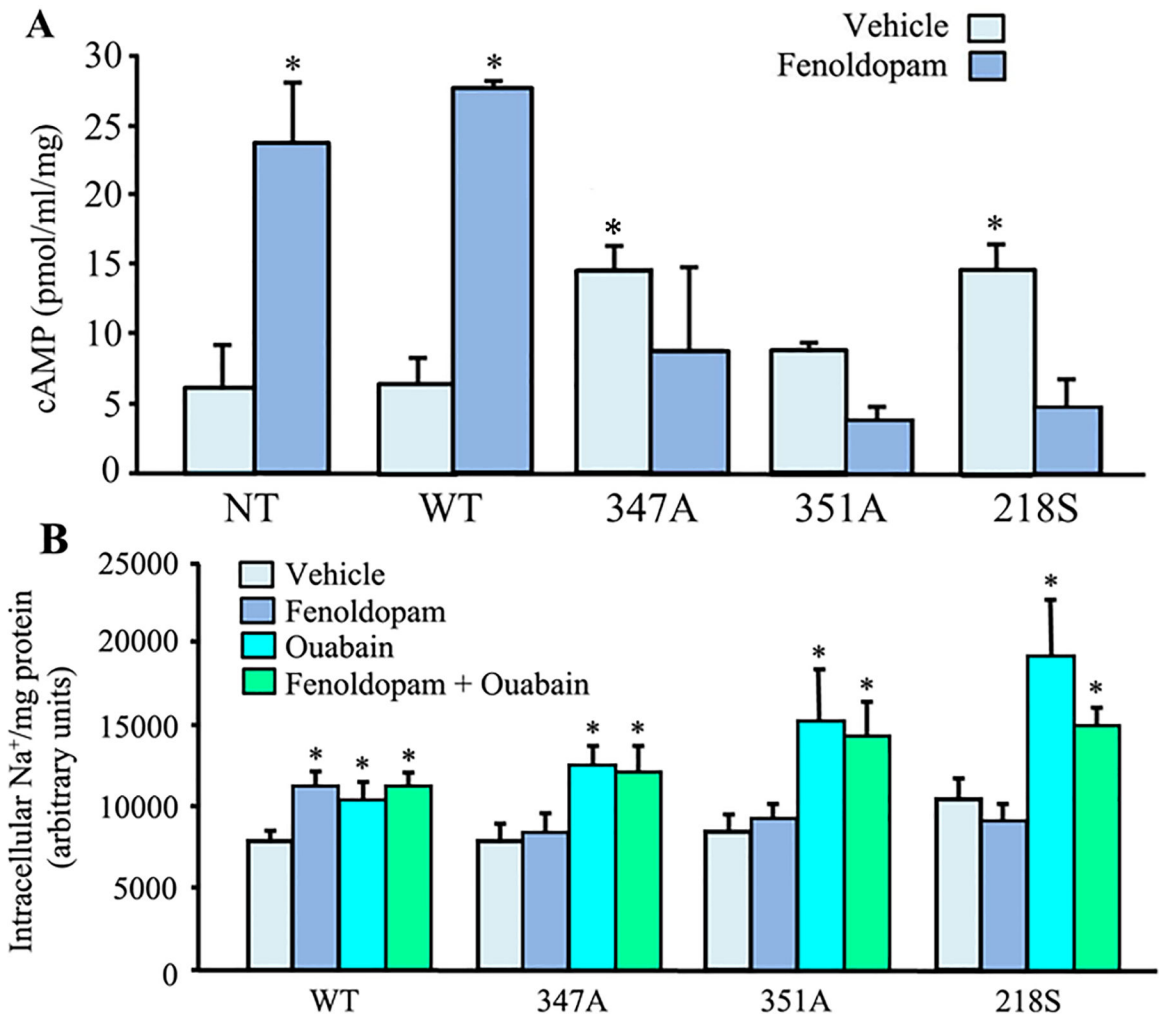

Figure 5. D_1R mutants have impaired activity.

A: The cells were serum-starved and pre-treated with IBMX for 2 hr before fenoldopam (1 μM) or vehicle treatment for 30 min to determine the cAMP response. The data were normalized for protein concentration. **B:** The hRPTCs were grown under polarized conditions on Transwells® to 100% confluence. The cells were serum-starved and pre-treated with the Na^+-K^+/ATPase (NKA) inhibitor ouabain for 60 min prior to 30-min fenoldopam treatment. Both treatments were given at the basolateral compartment. Intracellular sodium was measured using sodium green assay and the data were normalized for protein concentration. NT= non-transfected hRPTCs; WT=D_1R wild-type transfected hRPTCs; 347A, 351A, and 218S are hRPTCs transfected with the corresponding D_1R mutants. *P<0.05, *vs.* vehicle-treated D_1R-WT (Figures 5A and 5B) or NT hRPTCs (Figure 5A), one-way ANOVA and Holm-Sidak post-hoc test, n=4–5/group.

Author Manuscript Author Manuscript Author Manuscript Author Manuscript

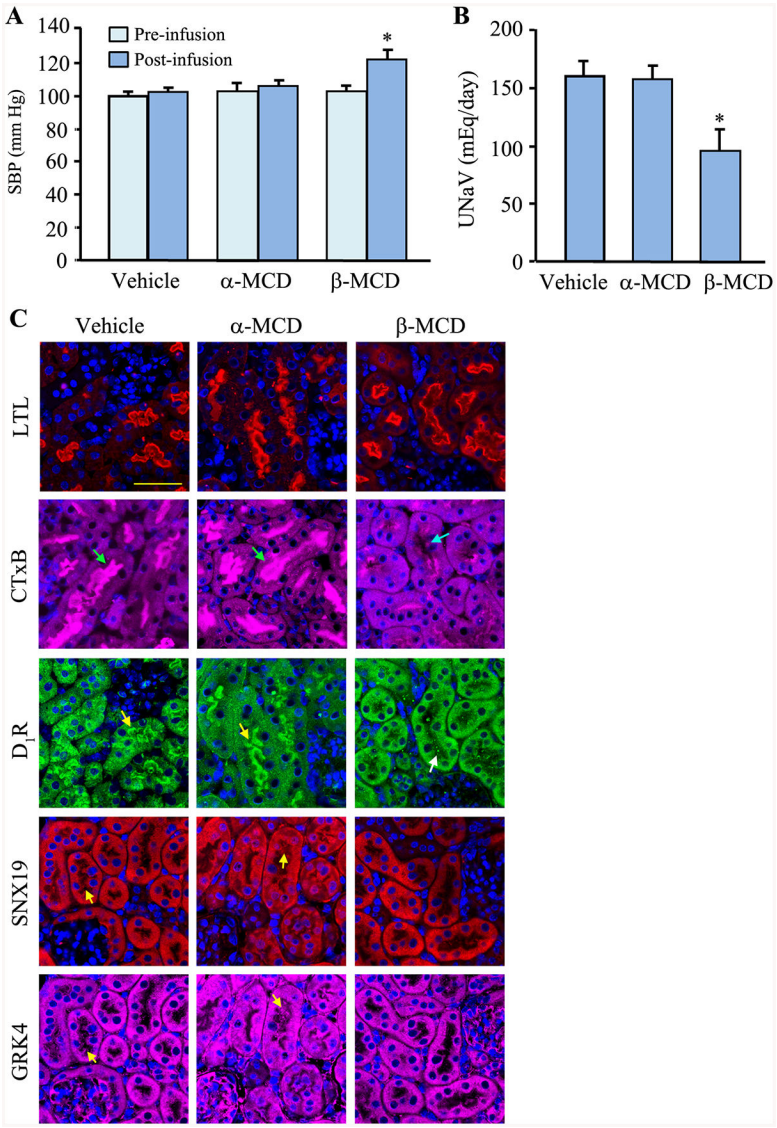

Figure 6. Disruption of lipid rafts only in the kidneys of C57BL/6J mice results in hypertension and impaired sodium excretion.

Adult (8–10 wk) male C57BL/6J mice on normal salt (0.8% NaCl) diet were uninephrectomized prior to a 7-day renal subcapsular minipump infusion of the cholesterol depletor β-MCD to disrupt the lipid raft. α-MCD and vehicle were used as negative controls. **A** & **B:** The mice were housed individually in metabolic cages to collect 24-hr urine samples on the 6th day after the start of the drug/vehicle treatment. Blood pressure was measured under pentobarbital anesthesia on the 7th day. **C:** The mice were sacrificed, and the kidneys were flash frozen in isopentane, fixed with 4% paraformaldehyde, sectioned, and immunostained. The brush border (using *Lotus tetragonolobus* Lectin, LTL), lipid raft (using cholera toxin subunit B, CTxB, green arrows), D_1R (yellow arrows), SNX19 (yellow arrows), GRK4 (yellow arrows), and nuclei (using DAPI) were visualized via confocal microscopy. Three to 4 mice per group and 630x magnification, scale bar = 20 μm

Author Manuscript Author Manuscript Author Manuscript Author Manuscript

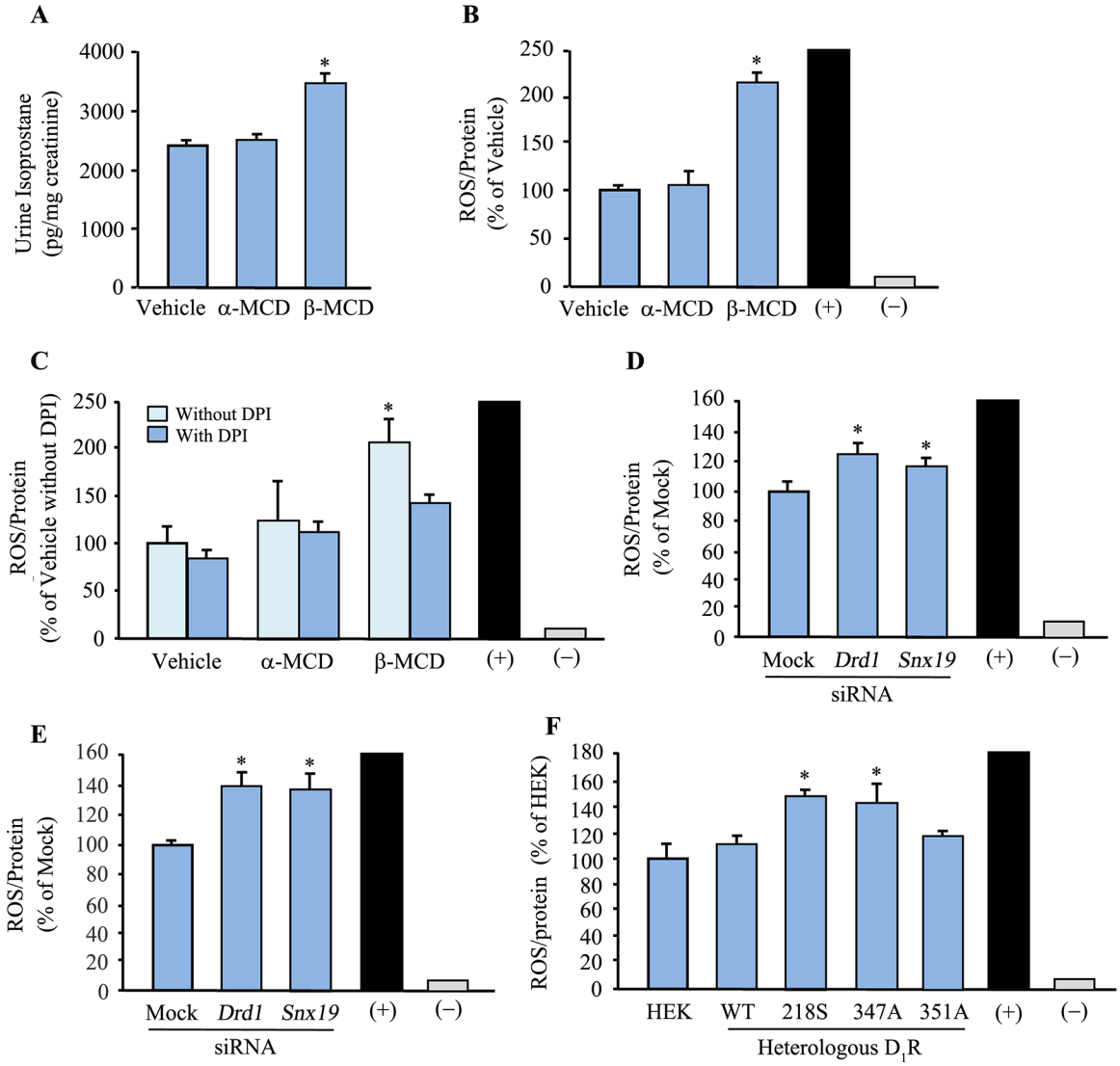

Figure 7. D_1R mutants cause oxidative stress.

A: Urine isoprostanes were measured and normalized for urine creatinine to determine the presence of oxidative stress in uninephrectomized adult male C57BL/6J mice on normal salt (0.8% NaCl) diet that received a 7-day renal-restricted lipid raft disruption via a renal subcapsular minipump infusion of the lipid raft disruptor β-MCD. α-MCD and vehicle were used as controls. (+) = 1% H_2O_2, (–) = without ROSstart. **B** and **C:** ROS production in mouse RPTCs treated with β-MCD, or α-MCD and vehicle as controls, for 2 hr. ROS was measured using ROSstart™ 650. In another set of experiments, diphenyleneiodonium (DPI; a NOX inhibitor) was used to determine if the increased ROS production was due to enhanced NOX activity. *P<0.05, *vs.* vehicle, α-MCD, or with DPI, one-way ANOVA and Holm-Sidak post-hoc test, n=3/group. (+, positive control, 200–250 ± 10% *vs.* vehicle) = 1% H_2O_2, (-, negative control) = without ROSstart. **D** and **E:** ROS production in mouse (**D**) and human (**E**) RPTCs in which *DRD1* or *SNX19* was silenced using siRNA. Non-silencing "Mock" siRNA was used as control. ROS was measured via ROSstart™ 650. *P<0.05, *vs.* Mock, one-way ANOVA and Holm-Sidak post-hoc test, n=3/group. (+, positive control,

Author Manuscript Author Manuscript Author Manuscript Author Manuscript

200–250 ± 10% *vs.* vehicle) = 1% H_2O_2, (-, negative control) = without ROSstart. **F:** ROS production in HEK-293 cells transfected with human D_1R-WT or mutants for 72 hrs. ROS was measured with ROSstart™ 650. *P<0.05, *vs.* untransfected HEK293 (HEK), human D_1R-WT (WT), or ΔD_1R-351A (351A), one-way ANOVA and Holm-Sidak post-hoc test, n=3/group. (+, positive control, 200–250 ± 10% *vs.* vehicle) = 1% H_2O_2, (-, negative control) = without ROSstart

Author Manuscript Author Manuscript Author Manuscript Author Manuscript

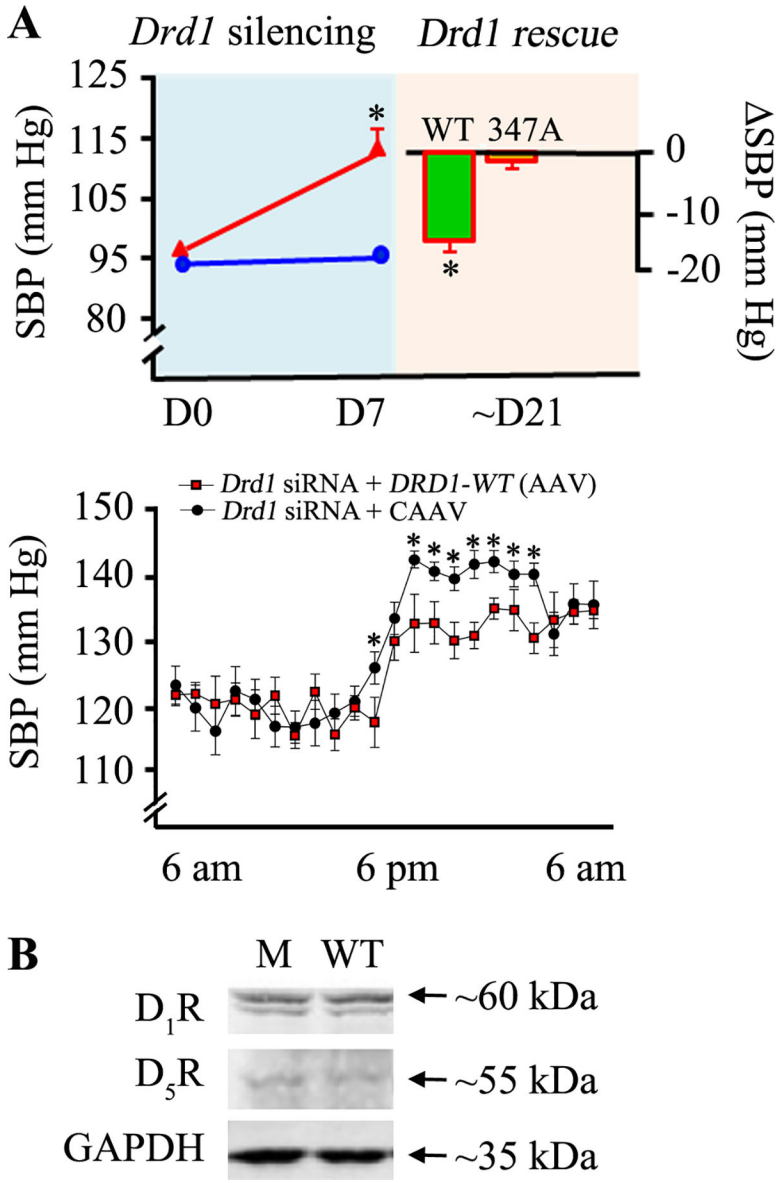

Figure 8. Renal tubule-restricted *DRD1* gene rescue using D_1R-WT, but not 347A mutant, normalizes the hypertension in renal-restricted D_1R-depleted C57BL/6J mice.

A: A 7-day (D7) renal subcapsular infusion of *Drd1* siRNA (red), but not of non-silencing "Mock" siRNA (blue), to the kidney of C57BL/6J increased the systolic blood pressure (SBP) measured under anesthesia (**top figure**). A renal tubule-restricted rescue using D_1R-WT but not D_1R 347A mutant, subcloned in AAV vectors normalized the blood pressure at day 21 (D21) in the mice with renal-restricted *Drd1* silencing (red). Baseline, before *Drd1* silencing = day 0 (D0), *P<0.05, *Drd1* siRNA *vs.* mock or WT *vs.* 347A post-rescue, Student's *t*-test. Blood pressure was also monitored via telemetry in conscious mice (**bottom figure**). *Rescue of with wild-type D_1R (*Drd1* siRNA + *DRD1-WT* [AAV]) blunted the increase in nighttime BP induced by renal-restricted D_1R silencing (*Drd1* siRNA). Shown are the values for the last week of siRNA treatment and the last week of *Drd1* siRNA + CAAV (control) and *Drd1* siRNA + *DRD1-WT* (AAV). *P<0.05, *vs.* mice treated with *Drd1*

siRNA + CAAV. **B**. Immunoblotting of renal D_1R, D_5R, and GAPDH. M = ΔD_1R-347A, WT = D_1R-WT.

Author Manuscript Author Manuscript Author Manuscript Author Manuscript

Author Manuscript Author Manuscript Author Manuscript Author Manuscript

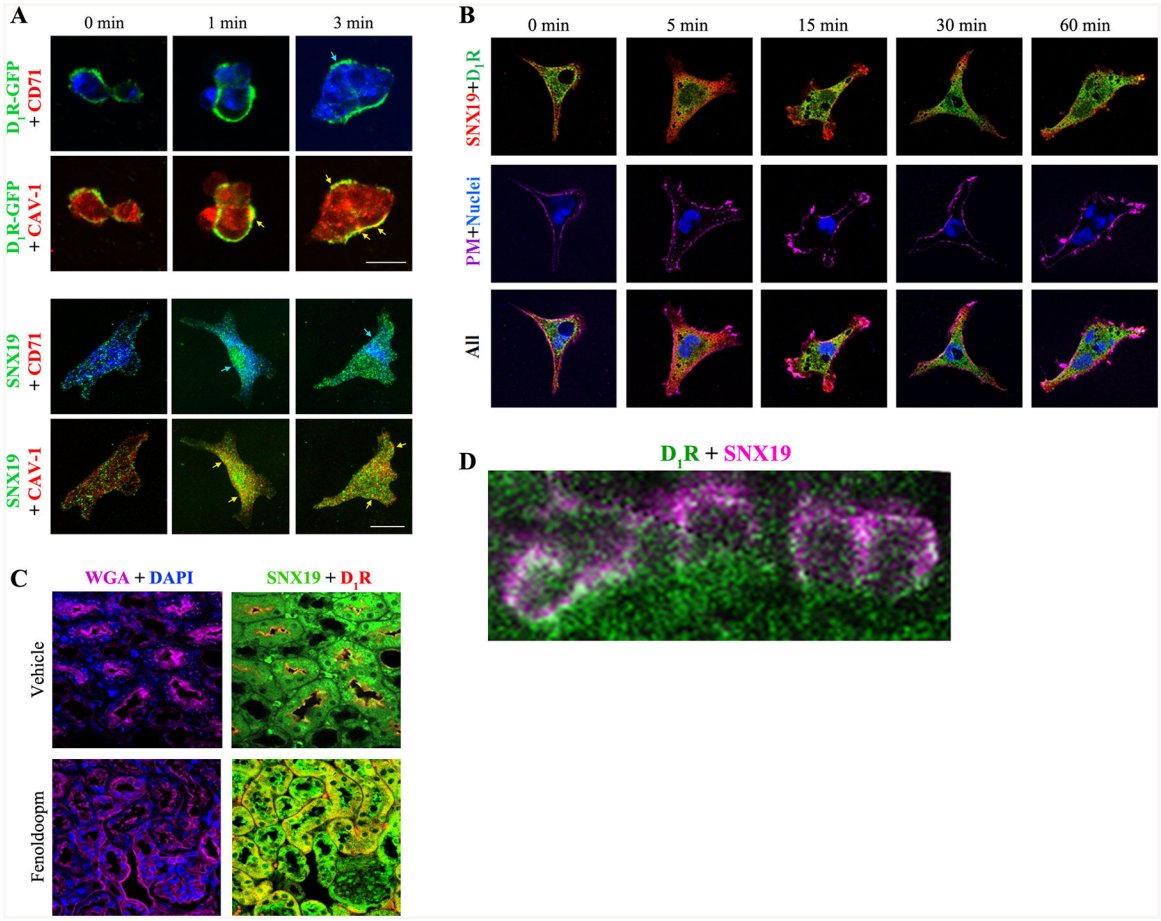

Figure 9. D_1R-GFP and SNX19 are expressed in lipid raft and non-raft domains.

A: The colocalization of D_1R-GFP with CAV-1 (lipid raft marker, arrows) and SNX19 with CAV-1 and, to a lesser degree, to CD71 (non-raft domain marker, arrows) is increased by fenoldopam (1 μM, 1 & 3 min). Images were obtained via laser confocal microscopy. 630x magnification, bar scale = 10 μm. **B:** Fenoldopam (D_1-like receptor agonist,1 μM) internalized and increased the colocalization of D_1R and SNX19 at 5 min & returned to 0 min position after 60 min in RPTCs. **PM**=plasma membrane. **C**: D_1R and SNX19 basally co-localized in RPTs of untreated mouse kidney ("vehicle"). Fenoldopam (2 μg/kg/min/5 min) increased the co-localization of D_1R and SNX19 in the cytosol of mouse RPTs. WGA= wheat germ agglutinin, plasma membrane marker. DAPI=nucleus. **D:** Colocalization of D_1R (pseudocolored green) and SNX19 (pseudocolored magenta) at the plasma membrane of renal proximal tubule of C57BL/6J mouse on normal salt diet (0.8% NaCl, 7 days) is denoted by the white circumscribed areas. The composite image was obtained via STED microscopy

Author Manuscript Author Manuscript Author Manuscript Author Manuscript

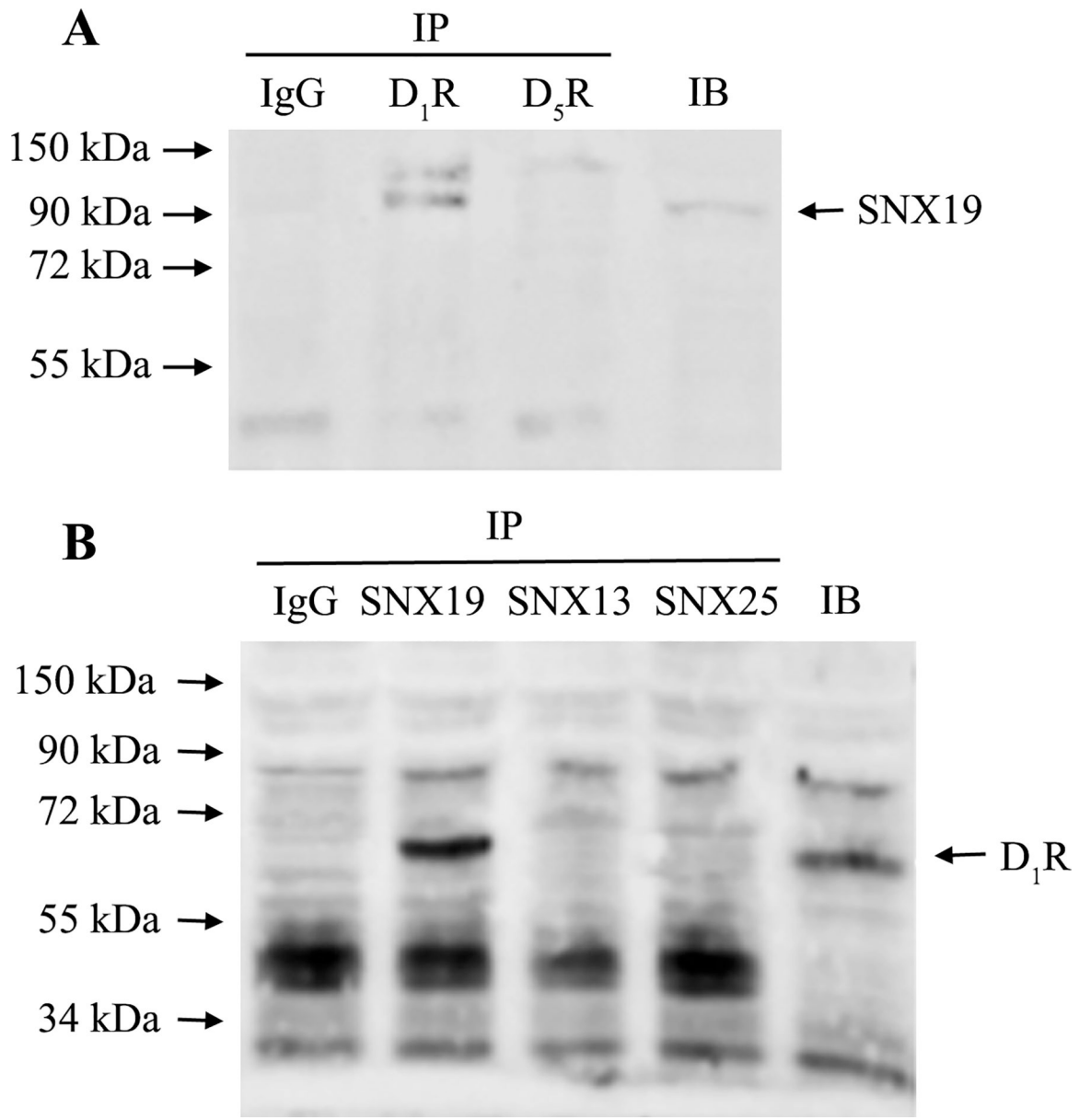

Figure 10. D_1R, not D_5R, co-immunoprecipitates (IP) with SNX19 (Figure A).
Reverse co-IP shows that SNX19, but not SNX13 or SNX25, co-IPs with D_1R (Figure 10B). Negative control = Co-IP with IgG from host that generated the antibody. IB=regular immunoblot.

Author Manuscript Author Manuscript Author Manuscript Author Manuscript

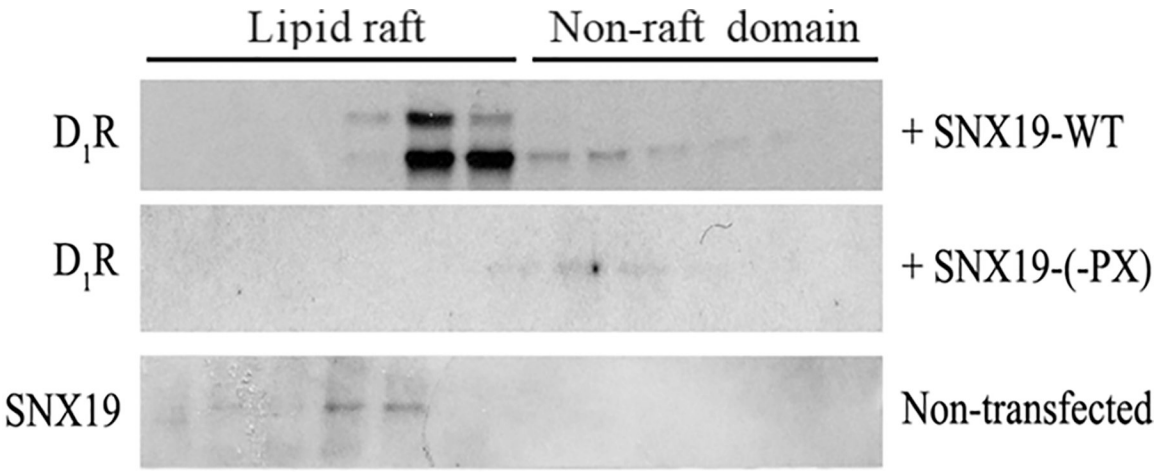

Figure 11. SNX19 mutants prevent D_1R partitioning to the lipid raft.

hRPTCs were transfected with the FLAG-tagged wild-type SNX19 (SNX19-WT) or mutant SNX19-(-PX). Similar to the D_1R studies, sucrose gradient ultracentrifugation was performed, and the 12 fractions were immunoblotted for endogenous D_1R. Endogenous SNX19 was also prepared from non-transfected hRPTCs.

Author Manuscript Author Manuscript Author Manuscript Author Manuscript

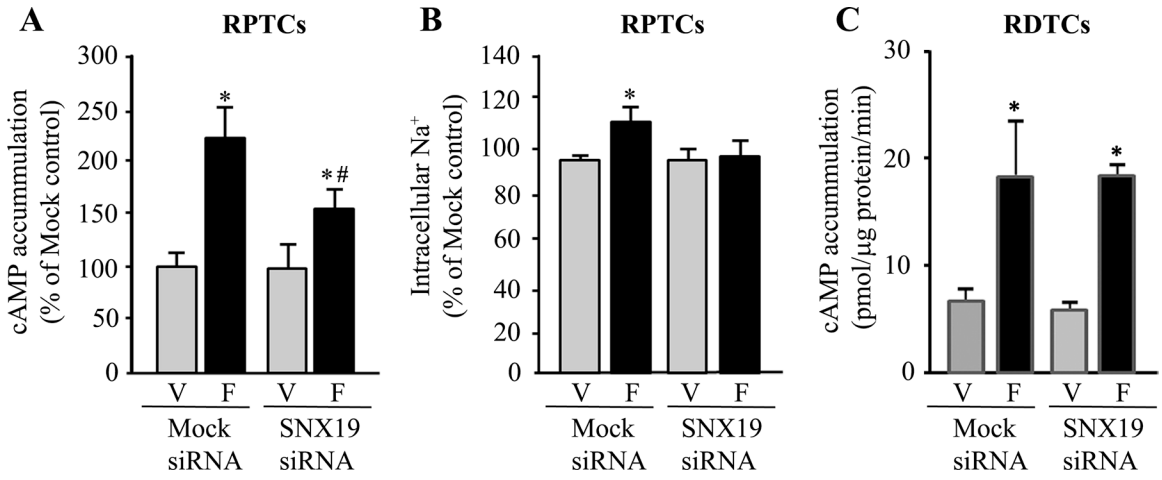

Figure 12. Effects of SNX19 silencing on cAMP production and Na^+ transport in human renal proximal and renal distal tubule cells.

SNX19 siRNA treatment blunted cAMP production (Figure 12A) and intracellular Na^+ (Na^+ green) accumulation (Figure 12B) in human RPTCs treated with the D_1-like receptor agonist fenoldopam (F; 1 μM/15 min). $^{\#}P<0.05$ *vs.* vehicle (V), SNX19 siRNA, *P<0.05 *vs.* vehicle non-silencing "Mock" or *SNX19* siRNA, one-way ANOVA, Holm-Sidak post-hoc test, n=4–5/group. Silencing of *SNX19* in human distal convoluted tubule cells (RDTCs) (Figure 12C) did not affect the ability of the D_1-like receptor agonist fenoldopam (Fen, 1 μM/15 min) to stimulate cAMP production. n=6/group

Author Manuscript Author Manuscript Author Manuscript Author Manuscript

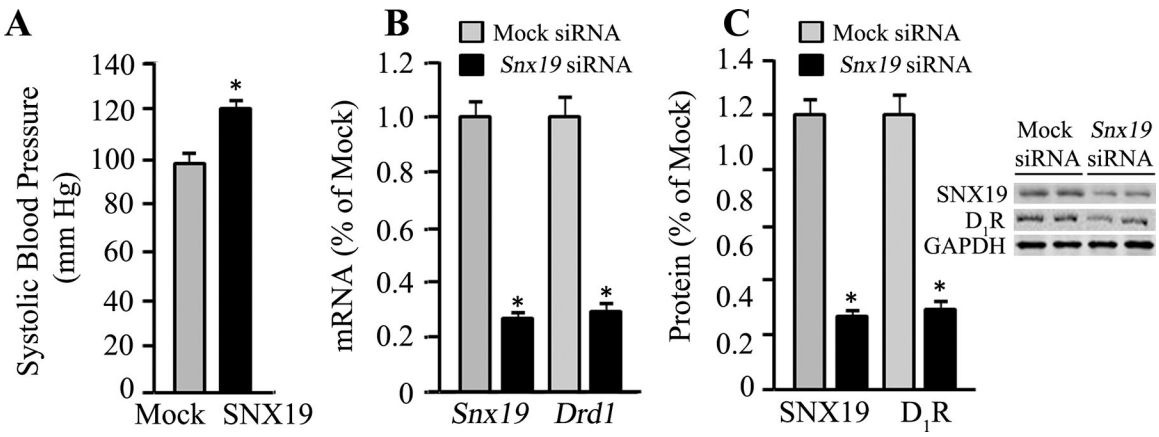

Figure 13. Effects of renal-restricted *Snx19* silencing on blood pressure and renal D_1R expression in C57BL/6J mice.

siRNA-mediated silencing of *Snx19* in the kidney of C57BL/6J mice on normal salt diet (0.8% NaCl) increased blood pressure (Figure 13A) and decreased renal *Drd1* mRNA (Figure 13B) and protein (Figure 13C) expressions. *P<0.05, vs. non-silencing "Mock" siRNA, Student's *t*-test, n=3–4/group. GAPDH was used as housekeeping gene for gene expression.

Author Manuscript Author Manuscript Author Manuscript Author Manuscript

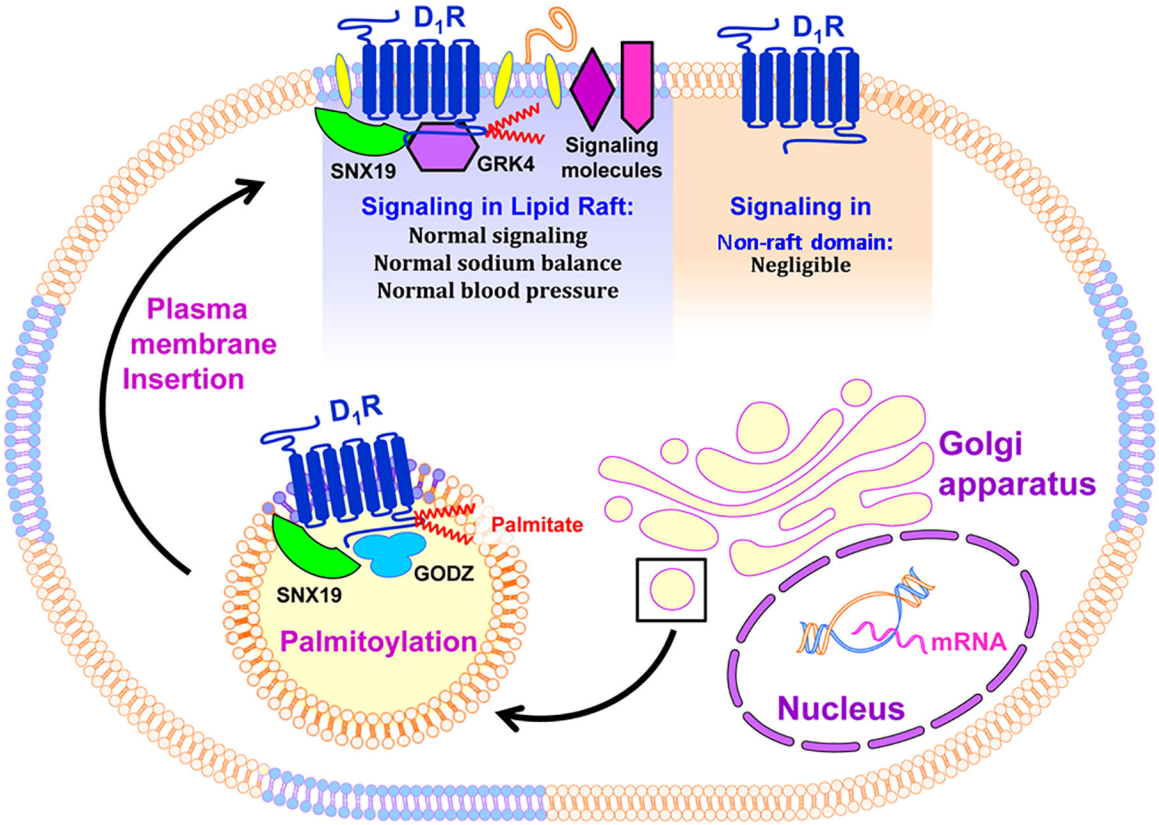

Figure 14. Palmitoylated D_1R in lipid raft microdomains.

Nascent D_1R undergoes post-translational modification at the Golgi apparatus. This includes palmitoylation of the cysteine residues at positions 347 and 351 found at the C-terminus through the GODZ enzyme, a process that may be facilitated by the adaptor protein SNX19. Palmitoylation promotes the partitioning of the receptor into the lipid raft where other components of the signal transduction pathway are localized, including the GRK4, G proteins, β-arrestins, adenylyl cyclases, other receptors, and effector proteins, such as the NOX and NKA, for normal signal transduction and appropriate cellular response. Negligible signaling may occur in the non-raft domains where some of the signaling molecules are missing in the case of the D_1R.